

# Comprehensive characterization of three classes of *Arabidopsis* SWI/SNF chromatin remodelling complexes

Received: 8 February 2022

Jing Guo<sup>1,2</sup>, Guang Cai<sup>2</sup>, Yong-Qiang Li<sup>2</sup>, Yi-Xuan Zhang<sup>2</sup>, Yin-Na Su<sup>1,2</sup>, Dan-Yang Yuan<sup>2</sup>, Zhao-Chen Zhang<sup>2</sup>, Zhen-Zhen Liu<sup>2</sup>, Xue-Wei Cai<sup>2</sup>, Jing Guo<sup>2</sup>, Lin Li<sup>2</sup>, She Chen<sup>2,3</sup> & Xin-Jian He<sup>1,2,3</sup>✉

Accepted: 19 October 2022

Published online: 5 December 2022

 Check for updates

Although SWI/SNF chromatin remodelling complexes are known to regulate diverse biological functions in plants, the classification, compositions and functional mechanisms of the complexes remain to be determined. Here we comprehensively characterized SWI/SNF complexes by affinity purification and mass spectrometry in *Arabidopsis thaliana*, and found three classes of SWI/SNF complexes, which we termed BAS, SAS and MAS (BRM-, SYD- and MINU1/2-associated SWI/SNF complexes). By investigating multiple developmental phenotypes of SWI/SNF mutants, we found that three classes of SWI/SNF complexes have both overlapping and specific functions in regulating development. To investigate how the three classes of SWI/SNF complexes differentially regulate development, we mapped different SWI/SNF components on chromatin at the whole-genome level and determined their effects on chromatin accessibility. While all three classes of SWI/SNF complexes regulate chromatin accessibility at proximal promoter regions, SAS is a major SWI/SNF complex that is responsible for mediating chromatin accessibility at distal promoter regions and intergenic regions. Histone modifications are related to both the association of SWI/SNF complexes with chromatin and the SWI/SNF-dependent chromatin accessibility. Three classes of SWI/SNF-dependent accessibility may enable different sets of transcription factors to access chromatin. These findings lay a foundation for further investigation of the function of three classes of SWI/SNF complexes in plants.

SWI/SNF (switch defective/sucrose non-fermentable) is a well-studied type of chromatin remodelling ATPase, which is mainly required for transcriptional activation in eukaryotes<sup>1</sup>. There are two SWI/SNF ATPases (Swi2 and Sth1) in yeast, one SWI/SNF ATPase (BRM) in *Drosophila* and two SWI/SNF ATPases (BRM and BRG1) in humans<sup>2</sup>. The SWI/SNF ATPases form two to three classes of multi-subunit complexes in yeast, *Drosophila* and mammals<sup>2–4</sup>. In plants, however, little is known

about the classification and composition of SWI/SNF complexes. In *Arabidopsis thaliana*, three types of SWI/SNF ATPase have been identified: BRAHMA (BRM/CHR2), SPLAYED (SYD/CHR3) and two closely related MINUSCULE1 (MINU1/CHR12) and MINUSCULE2 (MINU2/CHR23) (refs. <sup>5,6</sup>). These SWI/SNF ATPases are conserved in the ATPase domain but differ in domain structure at N-terminal and C-terminal regions<sup>7</sup>. The remarkable differences in the domain structure of the

<sup>1</sup>College of Life Sciences, Beijing Normal University, Beijing, China. <sup>2</sup>National Institute of Biological Sciences, Beijing, China. <sup>3</sup>Tsinghua Institute of Multidisciplinary Biomedical Research, Tsinghua University, Beijing, China. ✉e-mail: [hexinjian@nibs.ac.cn](mailto:hexinjian@nibs.ac.cn)

three types of *Arabidopsis* SWI/SNF ATPase suggest that they are functionally divergent.

The mutants of three types of *Arabidopsis* SWI/SNF ATPase display pleiotropic developmental defects, indicating that these ATPases are important for multiple developmental processes. The developmental defects of the *brm* and *syd* single mutants include a reduction in plant size, slow growth, curled rosette leaves, aberrant flower development and sterility<sup>8–11</sup>. *BRM* and *SYD* occupy thousands of common target genes and exhibit similar binding patterns, indicating that the two enzymes are functionally related<sup>12,13</sup>. The *brm syd* double mutant shows embryonic lethal phenotypes, with the embryo development arrested at the heart stage<sup>14</sup>. Loss-of-function *minu1* and *minu2* single mutants are morphologically indistinguishable from the wild type, while the *minu1/2* (*minu1* and *minu2*) double mutant exhibits embryonic lethal phenotypes<sup>15,16</sup>. The weak *minu1/2* double mutant forms small and bushy plants that have striking defects in maintenance of both root and shoot apical meristems<sup>17</sup>. These results suggest that the *Arabidopsis* SWI2/SNF2 ATPases have specific functions in regulating development, although the mechanisms underlying the specificity are largely unknown.

In addition to the SWI/SNF ATPases, the *Arabidopsis* SWI/SNF core subunits are thought to include four SWI3 proteins (SWI3A, SWI3B, SWI3C and SWI3D), two SWP73 proteins (SWP73A and SWP73B), two ARP proteins (ARP4 and ARP7) and a single SNF5 protein termed BUSHY (BSH)<sup>7,18–20</sup>. Previous studies have identified additional conserved *Arabidopsis* SWI/SNF subunits, including LEAF AND FLOWER RELATED (LFR), which shares similarity with the human BAF subunit BAF250 at Armadillo repeat (ARM-repeat)<sup>21</sup>; ANGUSTIFOLIA3 (AN3), which is an orthologue of the human SWI/SNF subunit SS18 (ref. <sup>20</sup>); BRM-INTERACTING PROTEINS 1 and 2 (BRIP1 and BRIP2), which are orthologues of the human SWI/SNF subunits GLTSCR1 and GLTSCR1L<sup>22</sup>; and BROMODOMAIN-CONTAINING PROTEIN1, 2 and 13 (BRD1, 2 and 13; BRD1/2/13) (refs. <sup>23,24</sup>). Although these *Arabidopsis* proteins have been identified as SWI/SNF subunits, whether and how they differentially interact with the SWI/SNF ATPases BRM, SYD and MINU1/2 are unclear. Classification, composition and functional mechanisms of SWI/SNF complexes remain to be illustrated in plants.

In this Article, we identified components of SWI/SNF complexes in *Arabidopsis* by affinity purification and mass spectrometry (AP-MS). On the basis of the AP-MS results, we identified three classes of *Arabidopsis* SWI/SNF chromatin remodelling complexes containing BRM, SYD or MINU1/2 as core enzymes, and named them as follows: BRM-associated SWI/SNF complexes (BAS), SYD-associated SWI/SNF complexes (SAS) and MINU-associated SWI/SNF complexes (MAS). We distinguished between the shared and unique subunits of the three classes of complexes in *Arabidopsis* and in *Oryza sativa*. We found that the three classes of *Arabidopsis* SWI/SNF complexes have different functions in regulating development and gene transcription. We mapped the profiles of the three classes of *Arabidopsis* SWI/SNF complexes on chromatin, and determined the effect of SWI/SNF mutations on chromatin accessibility at the whole-genome level. These results provide insight into the molecular mechanisms underlying the functions of different SWI/SNF complexes in plants.

## Results

### Three classes of SWI/SNF complexes in *Arabidopsis*

To determine the composition of SWI/SNF ATPase-containing complexes in *Arabidopsis*, we performed AP-MS using transgenic plants expressing Flag-tagged BRM, SYD and MINU2. The AP-MS assay identified all previously known SWI/SNF subunits<sup>20,22–24</sup> (Fig. 1a, Supplementary Table 1 and Supplementary Data 1). In addition to the known subunits, several other proteins were co-purified with BRM, SYD and/or MINU2, and these proteins were considered to be candidates of newly identified SWI/SNF subunits (Fig. 1a). We generated transgenic plants expressing both the known and newly identified putative SWI/SNF

subunits tagged by Flag and then performed AP-MS to determine the classification and composition of SWI/SNF complexes. On the basis of these AP-MS assays, we identified a total of 35 SWI/SNF subunits that formed three classes of SWI/SNF complexes, which we termed BAS, SAS and MAS (BRM-, SYD- and MINU1/2-associated SWI/SNF complexes) (Fig. 1a,b).

We identified these SWI/SNF subunits in at least one of the three classes of SWI/SNF complexes (Fig. 1a, Supplementary Table 1 and Supplementary Data 1). BCL7A, BCL7B, ARP4, APR7 and SWP73B are conserved subunits that are shared by all three classes of SWI/SNF complexes (Fig. 1a,b). As determined by the AP-MS data from the current study (Supplementary Data 1) and previous studies<sup>25–28</sup>, ARP4 is a shared subunit of SWI/SNF, INO80, SWR1 and NuA4 complexes, whereas ARP7 is a shared subunit of different SWI/SNF complexes but not of the other complexes. AN3, a homologue of the human SWI/SNF subunit SS18, was previously shown to interact with SWI/SNF complex components<sup>20</sup>. Our AP-MS result indicated that AN3 and its paralogues GIF2 and GIF3 are subunits of BAS and SAS but not of MAS. LFR was recently shown to interact with the SWI/SNF component SWI3B<sup>29</sup>. Our AP-MS data showed that LFR interacts not only with SWI3B but also with SWI3A and SWI3D, and is a shared subunit of SAS and MAS (Fig. 1a,b). BRM, SWI3C, SWP73A, BRIP1/2 and BRD1/2/13 are unique subunits of BAS; SYD, SWI3D and the newly identified plant-specific homologous subunits SYS1 (SAS subunit 1), SYS2 and SYS3 are unique subunits of SAS; SWI3A, SWI3B, BSH and newly identified subunits including SAWADEE homeodomain homologue 2 (SHH2), PHD-containing MAS subunits (PMS1A, PMS1B, PMS2A and PMS2B), MINU-interacting subunit (MIS), small subunit of MAS (SSM) and the bromodomain-containing protein BRD5 are unique subunits of MAS (Fig. 1a,b). These AP-MS results have revealed both shared and unique subunits of the three classes of SWI/SNF complexes in *Arabidopsis*.

### Three classes of SWI/SNF complexes in rice

As indicated by phylogenetic analysis, the *Arabidopsis* SWI/SNF ATPases BRM, SYD and MINU1/2 are conserved in plants (Extended Data Fig. 1a). To determine whether the three classes of SWI/SNF complexes are conserved in plants, we generated GFP-tagged transgenes expressing representative SWI/SNF subunits in *Oryza sativa* and identified proteins co-purified with these SWI/SNF subunits. OsDEC, OsCHB704 and OsBSH, which are orthologous to the BAS subunits BRIP1/2, the SAS subunit SWI3D and the MAS subunit BSH, respectively, were chosen as bait proteins for AP-MS in rice (Supplementary Table 2). As determined by AP-MS, OsDEC, OsCHB704 and OsBSH interact with orthologues of BAS-, SAS- and MAS-specific subunits, respectively, while all of them interact with orthologues of BAS/SAS/MAS-shared subunits (Extended Data Fig. 1b,c and Supplementary Data 2). OsBCL7, an orthologue of the *Arabidopsis* BAS/SAS/MAS-shared subunits BCL7A/B, interacts not only with BAS/SAS/MAS-shared subunits but also with subunits that are unique to each of the three classes of SWI/SNF complexes; OsLFR, an orthologue of the *Arabidopsis* SAS/MAS-shared subunit LFR, interacts with both SAS subunits and MAS subunits but not with BAS subunits (Extended Data Fig. 1b,c and Supplementary Data 2). These results suggest that the three classes of SWI/SNF complexes are conserved in rice. We compared the SWI/SNF complex subunits in yeast, *Drosophila*, human, *Arabidopsis* and rice (Supplementary Table 3). Although core subunits are shared by all of the SWI/SNF complexes in the different species, the existence of different accessory subunits distinguishes the SWI/SNF complexes in these species. In particular, we identified several plant-specific subunits, including SYS1, SYS2 and SYS3 in the SAS complex as well as MIS, SSM and SHH2 in the MAS complex.

### Interactions of SWI/SNF components determined by Y2H

We performed yeast two-hybrid (Y2H) to determine protein–protein interactions among subunits of each SWI/SNF complex. In total, the Y2H assay identified 90 protein–protein interactions (Extended Data

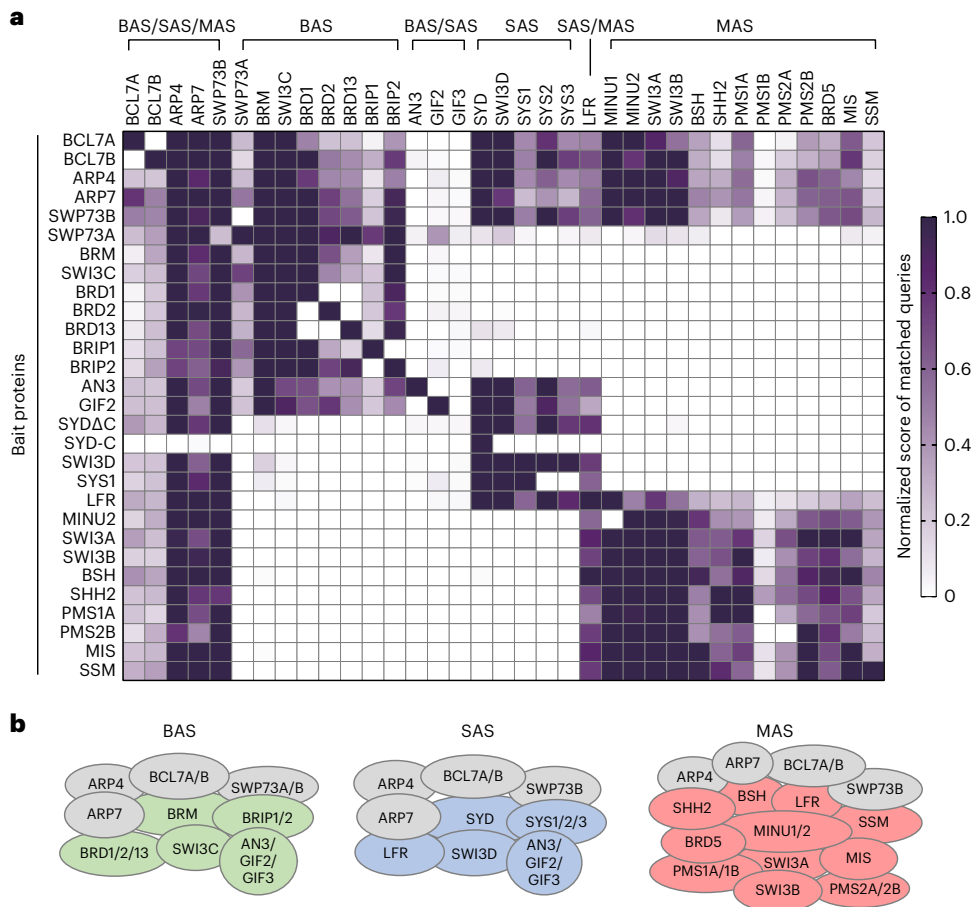


**Fig. 1 | Identification and classification of SWI/SNF complexes in *Arabidopsis*.** **a**, Heat map visualization of proteins co-purified with Flag-tagged *Arabidopsis* SWI/SNF subunits as determined by AP-MS. The matched queries of a prey protein are normalized by the average matched queries of the total subunits

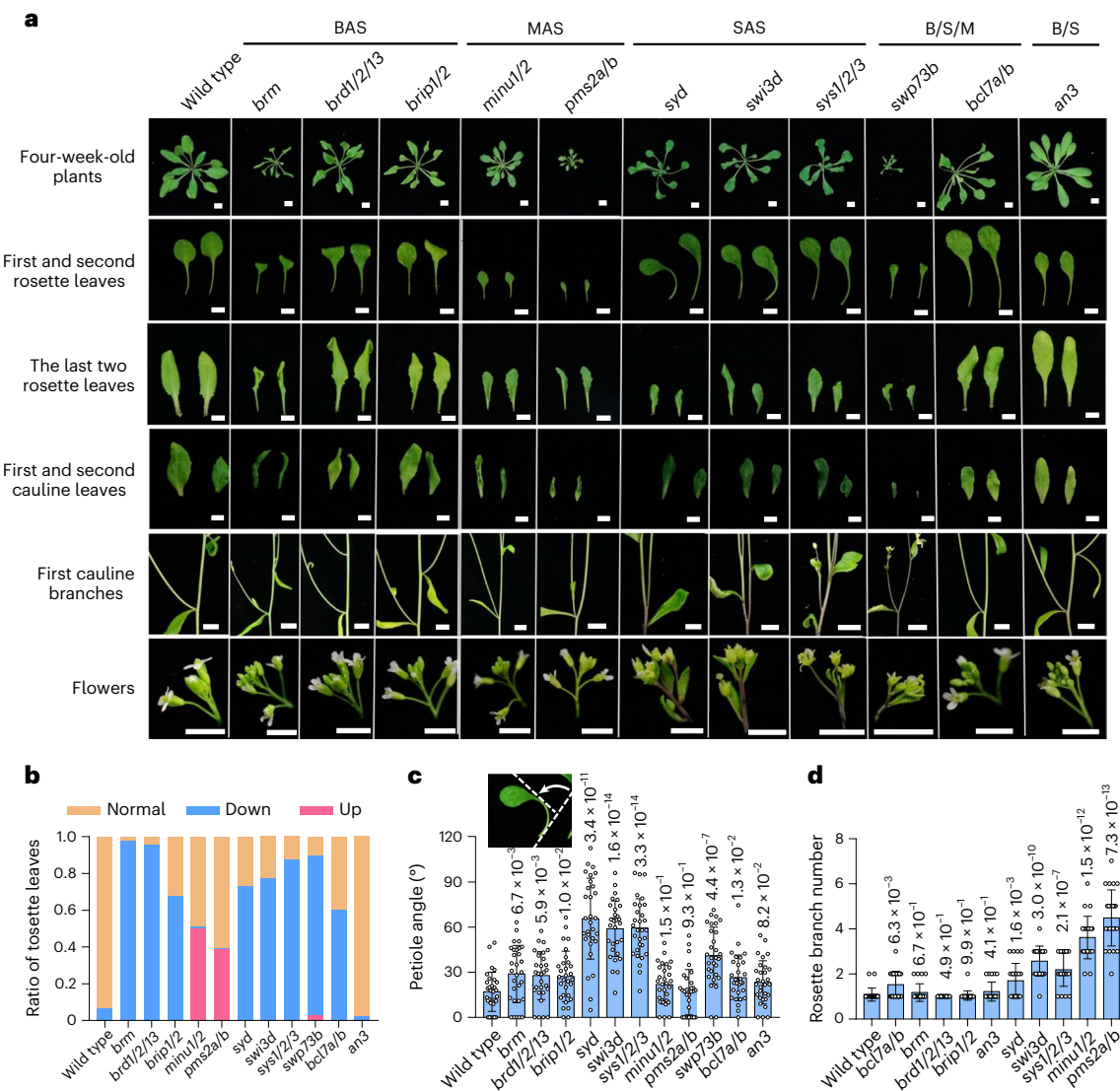
purified by a bait protein. **b**, Schematics depicting compositions of *Arabidopsis* BAS, SAS and MAS complexes. Shared subunits are shown in grey. Specific subunits of BAS, SAS and MAS complexes are shown in green, blue and red, respectively.

Fig. 2a–c), of which only 27 had been previously identified<sup>8,14,22–24,30–33</sup>. As indicated by the cryogenic electron microscopy structures of yeast and human SWI/SNF complexes<sup>34–36</sup>, the N-terminal domain of the SWI/SNF ATPases forms a module with most of the accessory subunits in the SWI/SNF complexes. By using truncated versions of BRM in Y2H, we found that the N-terminal domain of BRM (BRM-T1, 1–744 amino acids (aa) but not the other domains (BRM-T2, 718–1611 aa; BRM-T3, 1,596–2,193 aa) is responsible for its interaction with the other components of the BAS complex (Supplementary Fig. 1). SYD contains an uncharacterized C-terminal domain that is dispensable as determined by complementation testing<sup>37</sup>. In line with the latter inference, the C-terminal truncated version of SYD (SYDAC, 1–1,720 aa) is both necessary and sufficient for interaction with the other components of the SAS complex (Fig. 1a and Extended Data Fig. 2b). SWI3A, SWI3B, SWI3C and SWI3D can form homodimers, and SWI3A and SWI3B can form a heterodimer, as determined by our Y2H assay (Extended Data Fig. 2a–c), which is consistent with a previous study<sup>32</sup>. The SWI3A–SWI3B interaction was confirmed by our AP-MS result (Fig. 1a and Supplementary Data 1). The dimerization of SWI3 homologues was shown in the high-resolution structures of both yeast and human SWI/SNF complexes<sup>34–36,38,39</sup>, suggesting that the dimerization of SWI3 subunits is conserved in eukaryotes. These analyses suggest that the overall architecture of *Arabidopsis* SWI/SNF complexes is likely to be conserved with that of the SWI/SNF complexes in other eukaryotes. In addition, our Y2H results indicated that all of the newly identified plant-specific subunits interact with at least one

conserved subunit (Extended Data Fig. 2b), supporting the importance of these plant-specific subunits in the SWI/SNF complexes.

**Specific functions of each SWI/SNF complex in development**

In *Arabidopsis*, conserved SWI/SNF components were shown to regulate various developmental processes, including the development of leaves, gametophytes, embryos and flowers<sup>8–10,17,31,32,37</sup>. The identification of three classes of *Arabidopsis* SWI/SNF complexes prompted us to determine whether the different classes have specific functions in development. We generated 11 single, double or triple mutants for the three classes of SWI/SNF complexes, in which *brm*, *brd1/2/13* (*brd1 brd2 brd13*) and *brip1/2* (*brip1 brip2*) are BAS mutants; *minu1 minu2* and *pms2a/b* (*pms2a pms2b*) are MAS mutants; *sys1 sys2/3* (*sys1 sys2 sys3*) are SAS mutants; *an3* is the mutant of the BAS- and SAS-shared subunit; and *swp73b* and *bcl7a/b* (*bcl7a* and *bcl7b*) are the mutants of subunits shared by all three classes of SWI/SNF complexes (Extended Data Fig. 3a and Supplementary Fig. 2a,b). All the tested mutants showed obvious defects in morphological phenotypes (Fig. 2a–d and Extended Data Fig. 3b–g). The morphological defects in *brd1/2*, *brip1/2*, *pms2a/b*, *sys1*, *swi3d* and *bcl7a/b* mutants were restored by corresponding transgenes (Supplementary Fig. 3a–f), suggesting that the SWI/SNF components are required for normal plant development. By comparing the developmental phenotypes of these mutants, we attempted to identify specific functions of the three classes of SWI/SNF complexes.



**Fig. 2 | Different developmental defects of BAS, SAS and MAS mutants in leaves, branches and flowers.** **a**, Morphological phenotypes of 4-week-old plants (shoots were removed from some bolting plants to show the morphology of rosette leaves), the first and second rosette leaves, the last two rosette leaves, the first and second cauline leaves, the first cauline branches, and flowers in wild-type and mutant plants. Scale bar, 0.5 cm. **b**, Proportion of normal-, down- and up-curled leaves to total rosette leaves in the indicated genotypes.  $n = 20$ .

**c**, Angles of curved petioles of the first and second rosette leaves. The angle measurement is shown.  $P$  values determined by two-tailed Student's  $t$ -test or Welch's  $t$ -test indicate the difference between the mutants and the wild-type control.  $n = 30$ . Data are presented as mean  $\pm$  standard deviation (s.d.). **d**, The number of rosette branches.  $P$  values determined by two-tailed Mann–Whitney  $U$  test indicate the difference between the mutants and the wild-type control.  $n = 23$ . Data are presented as mean  $\pm$  s.d.

A downward-curving leaf phenotype was previously reported in the mutants of some conserved SWI/SNF components<sup>8,22–24,31,32</sup>, which we have now identified as subunits of BAS and SAS complexes. We found that, except for *an3*, all of the tested BAS and SAS mutants have a downward-curving phenotype in rosette leaves and cauline leaves, whereas none of the MAS mutants showed such a phenotype (Fig. 2a,b and Extended Data Fig. 3b). The lack of this phenotype in *an3* may be caused by the functional redundancy between AN3 and its paralogues (GIF2 and GIF3). Thus, the BAS and SAS complexes are specifically responsible for preventing the leaf from curling downward. The downward-curving phenotype appears in the BAS and SAS mutants but not in the MAS mutants *minu1/2* or *pms2a/b*, whereas the later-produced rosette leaves and early-produced cauline leaves in the MAS mutants are curved upward along the longitudinal axis (Fig. 2a and Extended Data Fig. 3b). The upward-curving leaves were also found in the mutants of SWI3B and LFR<sup>33,40,41</sup>, which have been identified as

MAS subunits in the current study, suggesting that the MAS complex is specifically responsible for preventing later-produced rosette leaves and early-produced cauline leaves from curving upward. Moreover, compared with the BAS and MAS mutants, the SAS mutants *syd*, *swi3d* and *sys1/2/3* have more early-produced rosette leaves with bent petioles (Fig. 2a,c and Extended Data Fig. 3b). These results demonstrate that the three classes of SWI/SNF complexes regulate leaf development in different ways.

The bushy appearance (as determined by the number of rosette branches) of the MAS mutants *minu1/2* and *pms2a/b* (Fig. 2d and Extended Data Fig. 3c) indicated that the MAS complex is required for maintaining normal plant branching. Compact inflorescences (as determined by cauline branching angles) were found in both the BAS/SAS/MAS shared mutant *bcl7a/b* and the SAS mutants *syd*, *swi3d* and *sys1/2/3* and to a lesser extent in the MAS mutants *minu1/2* and *pms2a/b* but not in any BAS mutants (Fig. 2a, Extended Data Fig. 3d and Supplementary

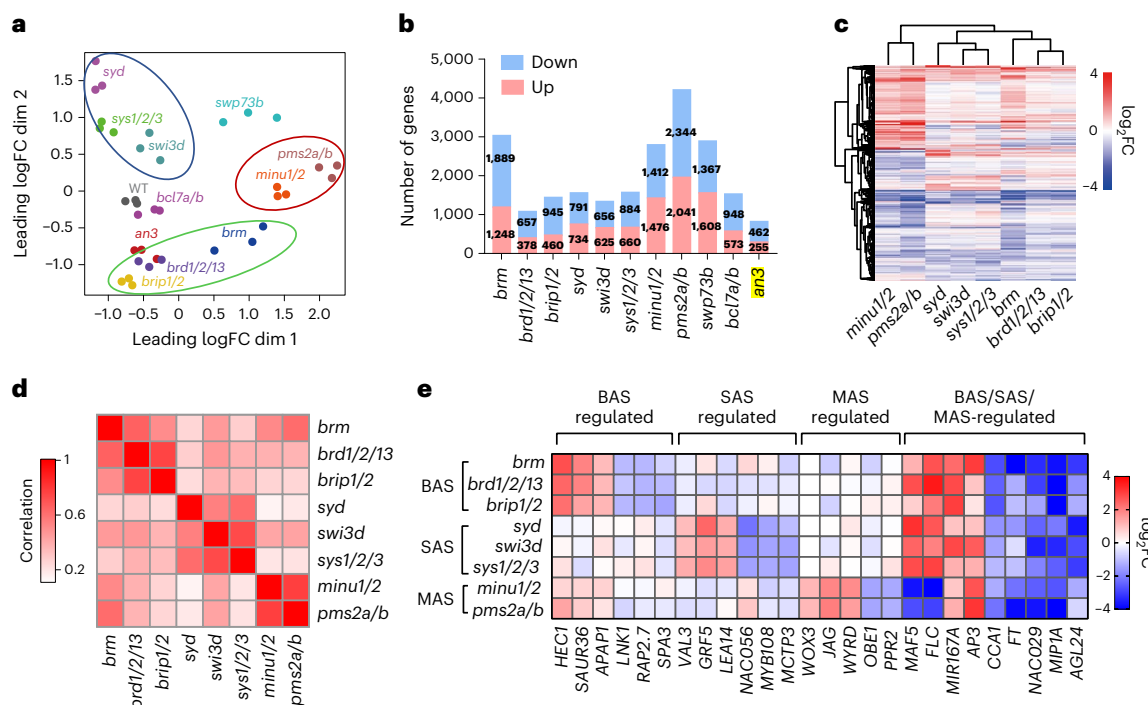


**Fig. 3 | BAS, SAS and MAS complexes function differently in regulation of gene expression.** **a**, MDS plot of the indicated RNA-seq samples. Clustering of BAS, SAS and MAS mutants is represented by green, blue and red circles. dim, dimension. **b**, Number of up- and downregulated genes in different mutants as determined by RNA-seq. **c**, Heat map showing hierarchical clustering of the total DEGs (7753) of *brm*, *brd1/2/13*, *brrip1/2*, *syd*, *swi3d*, *sys1/2/3*, *minu1/2* and *pms2a/b*.

Red and blue represent up- and downregulated genes, respectively. **d**, Heat map showing the pairwise Pearson correlation coefficient of *brm*, *brd1/2/13*, *brrip1/2*, *syd*, *swi3d*, *sys1/2/3*, *minu1/2* and *pms2a/b* based on expression changes of the total DEGs. **e**, Heat map showing the relative expression pattern of indicated development-related genes in BAS, SAS and MAS mutants. Red and blue represent up- and downregulated genes, respectively.

Fig. 3c), suggesting that the SAS complex is a major SWI/SNF complex that is responsible for maintaining proper angles of caulinine branching. Cauline branches of wild-type plants normally initiate at the axil of cauline leaves, and the SAS mutants *syd*, *swi3d* and *sys1/2/3* but not any other SWI/SNF mutants have a high ratio of cauline branches that initiate at the internode (Fig. 2a and Extended Data Fig. 3d), indicating that the SAS complex is required for the initiation of cauline branches at the axil. Splayed open floral buds were first reported in the *syd* mutant<sup>10</sup>; the same phenotype was found in the SAS mutants *syd*, *swi3d* and *sys1/2/3* and in the BAS/SAS/MAS-shared subunit mutant *syp73b* but not in the other mutants (Fig. 2a and Extended Data Fig. 3f), supporting the notion that the SAS complex has a specific function in regulating floral development. Siliques length was reduced to varying degrees in all of the tested SWI/SNF mutants (Extended Data Fig. 3g), suggesting that all three SWI/SNF complexes are involved in producing normal siliques, although the underlying mechanisms remain unknown. These analyses suggest that the three SWI/SNF complex classes have specific functions in regulating various developmental processes.

### Regulation of gene expression by different SWI/SNF complexes

To investigate how the three SWI/SNF complex classes differentially regulate development, we performed RNA deep sequencing (RNA-seq) in the wild type and the SWI/SNF mutants. Multidimensional scaling (MDS) analyses of RNA-seq data revealed a high reproducibility of three biological replicates for each genotype and indicated that the expression patterns of the mutants of the same SWI/SNF complex are similar to each other but differ from those of the mutants of the other SWI/SNF complexes (Fig. 3a–c). Differentially expressed genes (DEGs) relative to the wild type ( $|\log_2(\text{fold change (FC)})| \geq 1$ , false discovery rate  $< 0.05$ ; exact negative binomial test) were identified in the SWI/SNF

mutants (Fig. 3b). The numbers of DEGs were positively correlated with the severity of developmental defects in the SWI/SNF mutants (Fig. 3b and Extended Data Fig. 4a,b). We compared DEGs in the SWI/SNF mutants relative to the wild type and found that the DEGs are more closely correlated between the mutants of the same SWI/SNF complex than between the mutants of different SWI/SNF complexes (Fig. 3c,d). In fact, positive correlations were found between all pairwise SWI/SNF mutants. This suggests that, although the three SWI/SNF complex classes regulate unique target genes, they can also cooperate to regulate overlapping target genes.

Considering that the mutants of three SWI/SNF complex classes showed specific defects in development (Fig. 2a–d and Extended Data Fig. 3a–f), we determined whether the three classes of SWI/SNF complexes regulate specific developmental processes by differentially regulating gene expression. We analysed the effects of SWI/SNF mutations on the expression of genes related to specific developmental processes including the regulation of flowering time and the development of flowers, embryos and leaves. RNA-seq data showed that the expression levels of all these development-related genes were more correlated between the mutants of the same SWI/SNF complex than between the mutants of different complexes (Extended Data Fig. 4c–f and Supplementary Data 4), implicating that the three SWI/SNF complex classes regulate specific developmental processes by regulating different sets of development-related genes. Interestingly, our RNA-seq data indicated that the expression levels of the key flowering repressor *FLC* and its close parologue *MAF5* were reduced in the MAS mutants and were increased in the BAS and SAS mutants, although the expression level of the downstream florigen gene *FT* was reduced in all the tested SWI/SNF mutants (Fig. 3e), suggesting that the different SWI/SNF complexes are coordinated to regulate flowering time through more complicated mechanisms than previously thought<sup>8,42,43</sup>. Moreover, the

expression levels of well-known floral development-related genes, such as the flowering promotion gene *AGL24* (*AGAMOUS-LIKE 24*), the floral homeotic gene *AP3* (*APETALA 3*) and the circadian rhythm regulator gene *CCA1* (*CIRCADIAN CLOCK ASSOCIATED 1*), were reduced in all the SWI/SNF mutants tested (Fig. 3e and Supplementary Data 4). These results suggest that, although three classes of SWI/SNF complexes regulate different sets of development-related genes, they also cooperatively regulate a common set development-related genes.

### Genomic regions occupied by different SWI/SNF complexes

To compare the occupancy of chromatin by the three classes of SWI/SNF complexes at the whole-genome level, we performed chromatin immunoprecipitation followed by sequencing (ChIP-seq) for the BAS components BRD1 and SWI3C; the SAS components SYD, SWI3D and SYS1; and the MAS components MINU2 and PMS2B. A correlation analysis indicated that, while the ChIP-seq signals of components from the same complex were highly correlated with each other, the ChIP-seq signals of the BAS components were highly correlated with those of the SAS components but were weakly correlated with those of the MAS components, eventually forming three clusters exactly corresponding to the three classes of SWI/SNF complexes (Fig. 4a). Analysis of the ChIP-seq data identified thousands of peaks for each tested SWI/SNF component (Supplementary Data 5). Like the previously reported location of the SWI/SNF components<sup>13,44</sup>, all the tested SWI/SNF components are enriched at transcription start site (TSS)-flanking regions (Extended Data Fig. 5a,b). The distribution patterns are highly similar among components of the same SWI/SNF complex class but are obviously different between components of different SWI/SNF complex classes (Fig. 4b and Extended Data Fig. 5a,b). While the BAS components are enriched at the up- and downstream regions of the TSS at a comparable level, the SAS components are enriched more at the upstream region than at the downstream region, and the MAS components are enriched more at the downstream region than at the upstream region (Fig. 4b and Extended Data Fig. 5a,b).

We assigned the SWI/SNF component peaks to adjacent genes and determined the genes occupied by each SWI/SNF component. The BRD1-occupied genes identified in the current study highly overlap with those identified by a previous study<sup>23</sup>, suggesting that our ChIP-seq data are reliable (Extended Data Fig. 5c). As the SYD ChIP-seq data used in the current analysis were generated from *SYDAC-GFP* transgenic plants, we also performed the ChIP-seq using the available SYD antibody in wild-type plants and compared their ChIP-seq results. The comparison indicated that SYD-occupied genes identified in *SYDAC-GFP* transgenic plants highly overlap with those identified by SYD antibody in wild-type plants, although the quality of the former is higher than that of the latter (Extended Data Fig. 5c), indicating that the ChIP-seq data generated from *SYDAC-GFP* transgenic plants are reliable. We found that components of the same SWI/SNF complex share common target genes to a large extent (Extended Data Fig. 5c). As the ChIP-seq data of BRD1, SWI3C, SWI3D, SYS1, MINU2 and PMS2B are of a high quality, we designated the common genes occupied by BRD1 and SWI3C, by SWI3D and SYS1, and by MINU2 and PMS2B as BAS-, SAS- and MAS-occupied genes, respectively.

In total, we identified 9,084, 8,110 and 9,685 genes that are occupied by BAS, SAS and MAS, respectively (Fig. 4c). In line with the previous finding that BRM- and SYD-occupied genes highly overlap<sup>13</sup>, we found that 85% of the SAS-occupied genes overlap with the BAS-occupied genes (Fig. 4c). Although the MAS complex also shares a subset of target genes with the BAS and SAS complexes, 40% of the MAS-occupied genes are not bound by the BAS or SAS complexes (Fig. 4c), suggesting that the MAS complex binds to a different set of genes. Identification of SWI3A and SWI3B as specific MAS subunits prompted us to determine whether SWI3A co-occupies chromatin with the other MAS subunits. ChIP-seq data indicated that the distribution pattern of SWI3A is highly similar to that of the MAS subunits MINU2 and PMS2B

but is different from that of the BAS and SAS subunits (Supplementary Fig. 4a,b), which supports the notion that SWI3A and SWI3B are specific subunits of the MAS complex.

To further characterize the genes occupied by different SWI/SNF complexes, we plotted the ChIP-seq signals of SWI/SNF components at the genic region, and independently sorted the genes by the enrichment of BRD1, SYD and MINU2 signals for analysis of BAS-, SAS- and MAS-occupied genes, respectively (Fig. 4d and Extended Data Fig. 6a,b). We also divided all the enriched regions of SWI/SNF components into descending enrichment deciles of BRD1, SYD and MINU2, and then analysed the enrichment of other SWI/SNF components at each decile (Fig. 4e and Extended Data Fig. 6c,d). The results indicated that the enrichments of the BAS and SAS components are positively correlated with each other but are not related to the enrichments of the MAS components, which is visualized by the BAS, SAS and MAS peaks as shown in the genome browser (Fig. 4f). These results confirm that the BAS and SAS complexes primarily occupy a common set of genes and that the MAS complex can occupy many genes that are not occupied by the BAS and SAS complexes.

### Histone modification levels of SWI/SNF-occupied regions

We compared the histone modification levels of regions occupied by different SWI/SNF components using published ChIP-seq data for the histone modifications H3ac, H3K4me3 and H3K27me3 (refs. <sup>25,45,46</sup>). As compared with randomly selected genomic regions, the BAS-, SAS- and MAS-occupied regions have high levels of H3ac and H3K4me3, which are associated with the active transcription<sup>47,48</sup>, and have background (for BAS- and SAS-occupied regions) or even lower (for MAS-occupied regions) levels of H3K27me3, which is associated with the repression of transcription<sup>49</sup> (Extended Data Fig. 7a). By comparing the histone modifications levels of BAS-, SAS- and MAS-occupied regions, we found that the H3ac and H3K4me3 levels are the highest at MAS-occupied regions, intermediate at BAS-occupied regions and the lowest at SAS-occupied regions (Extended Data Fig. 7a). Given that the active histone modifications H3ac and H3K4me3 are mainly enriched at intragenic regions of protein-coding genes but not at distal promoter regions or at intergenic regions in *Arabidopsis*<sup>25,45,48</sup>, the different levels of active histone modifications at BAS/SAS/MAS-occupied regions are consistent with the different locations of these regions relative to the TSS as shown above (Fig. 4b and Extended Data Fig. 5a,b). Moreover, the expression levels of genes occupied by all the tested SWI/SNF components are higher than the expression levels of random genes; the expression levels of BAS- and SAS-occupied genes are comparable and are lower than the expression levels of MAS-occupied genes (Extended Data Fig. 7b). We further analysed the enrichments of H3ac, H3K4me3 and H3K27me3 at BAS-, SAS- and MAS-occupied regions by heat maps and by box plotting of descending deciles. The analyses indicated that the enrichments of H3ac and H3K4me3 are positively correlated with the enrichment of MAS but not with the enrichments of BAS and SAS, while the enrichment of H3K27me3 is weakly and negatively correlated with the enrichments of BAS and SAS, the H3K27me3 level is extremely low at MAS-occupied regions (Extended Data Fig. 7c,d). These results suggest that the MAS-occupied regions are more active than the BAS- and SAS-occupied regions.

We assessed whether unique subunits of the BAS and MAS complexes are responsible for the binding of the complexes to genes with more active histone modifications. The bromodomain-containing BAS subunit BRD13 and the bromodomain-containing MAS subunit BRD5 bind to acetylated histone<sup>50</sup>. Our pull-down and isothermal titration calorimetry (ITC) analyses indicated that the three homologous bromodomain-containing BAS subunits, that is, BRD1/2/13, bind to acetylated histone, and that the binding ability of BRD1 is eliminated by mutations of conserved residues (Y207A, N251A and Y258A) in the bromodomain (Extended Data Fig. 8a-d). We therefore infer that BRD1/2/3 and BRD5 are involved in the association of the BAS and MAS complexes

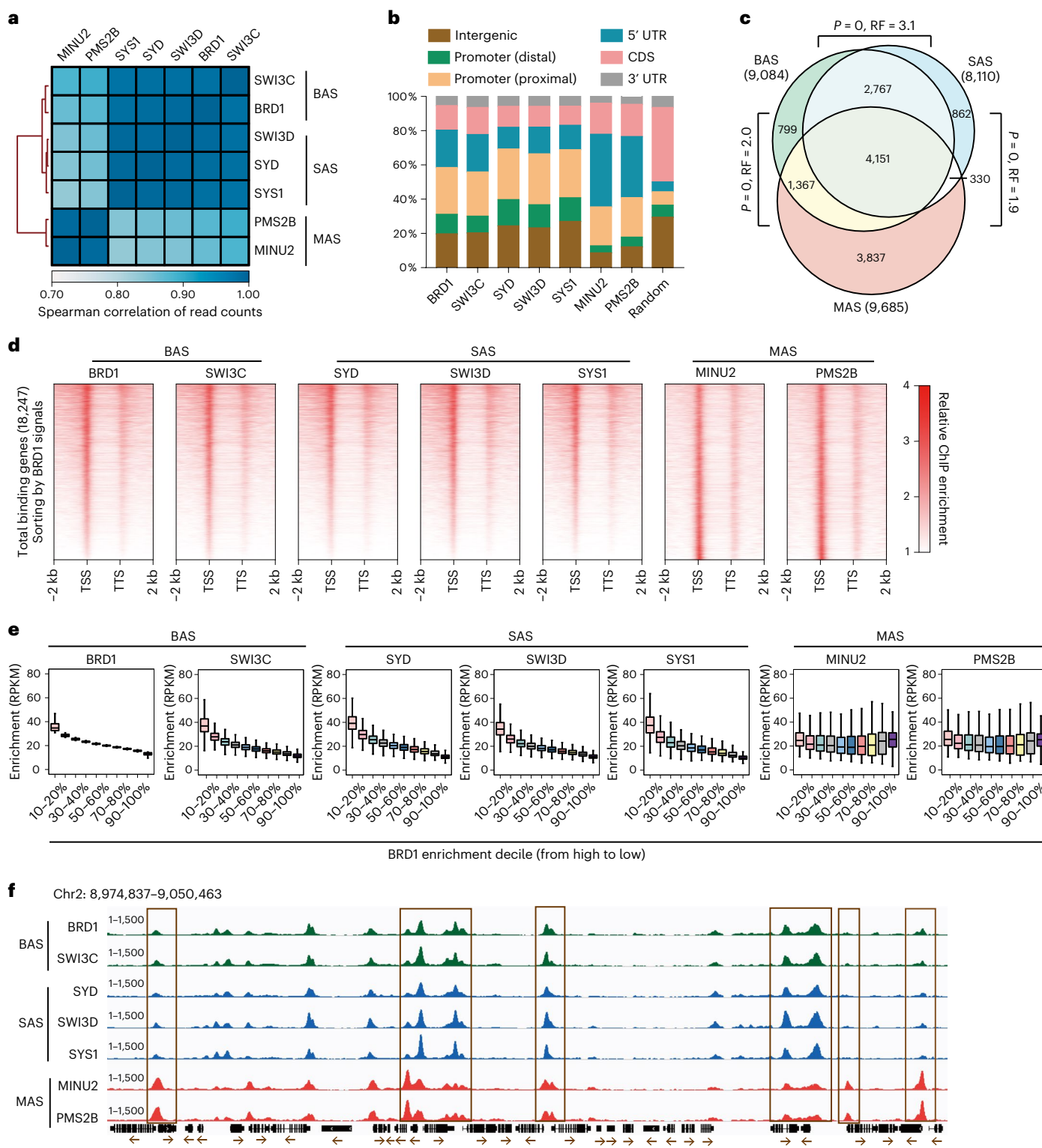


**Fig. 4 | Differential occupancy of BAS, SAS and MAS complexes on chromatin.** **a**, Heat map showing the pairwise Spearman correlation coefficient of ChIP-seq read counts between different SWI/SNF subunits. **b**, The proportion of peaks annotated to specified chromatin features. Distal promoter: -400–1,000 bp upstream of the TSS. Proximal promoter: -1–400 bp upstream of the TSS. Random: 8,000 random genomic sites. **c**, Venn diagram showing the overlap of BAS-, SAS- and MAS-bound genes.  $P$  values were determined by hypergeometric test (one-tailed). RF: representation factor (the number of overlapping genes divided by the expected number of overlapping genes drawn from two independent groups). **d**, Heat map showing the enrichment of indicated SWI/SNF components (BRD1, SWI3C, SYD, SWI3D, SYS1, MINU2, PMS2B) across genes sorted by maximum BRD1 enrichment value at these genes. TSS, transcription start site; TTS, transcription termination site. **e**, Enrichment of indicated SWI/SNF components at BRD1 enrichment deciles of the total regions ( $n = 18,552$ ) occupied by SWI/SNF components. In box plots, centre lines and box edges are medians and the interquartile range (IQR), respectively. Whiskers extend within 1.5 times the IQR. **f**, Snapshot showing the ChIP-seq signals of the SWI/SNF subunits at enriched regions. Peaks marked with brown boxes represent the genomic regions with differential occupancy of BAS, SAS and MAS complexes. The scale of normalized reads is shown.

SNF components at all the SWI/SNF components-occupied 18,247 genes. The genes are sorted by the maximum enrichment value of BRD1 at these genes. TSS, transcription start site; TTS, transcription termination site. **e**, Enrichment of indicated SWI/SNF components at BRD1 enrichment deciles of the total regions ( $n = 18,552$ ) occupied by SWI/SNF components. In box plots, centre lines and box edges are medians and the interquartile range (IQR), respectively. Whiskers extend within 1.5 times the IQR. **f**, Snapshot showing the ChIP-seq signals of the SWI/SNF subunits at enriched regions. Peaks marked with brown boxes represent the genomic regions with differential occupancy of BAS, SAS and MAS complexes. The scale of normalized reads is shown.

with histone acetylation-enriched chromatin. Although a putative bromodomain is present in the BAS catalytic subunit BRM, the bromodomain is not conserved in several critical residues (Extended Data Fig. 8a), and is unlikely to have the acetylated-histone binding ability. In addition, we found that the closely related MAS subunits PMS2A/B contain two PHD domains, among which the C-terminal PHD domain of PMS2A/B is similar to the well-characterized H3K4me3-binding PHD domains in the other proteins (Extended Data Fig. 8e,f,i)<sup>51–54</sup>. Our pull-down assay showed that PMS2B but not the distantly related PHD-containing MAS subunit PMS1A binds to H3K4me3 and that the binding is disrupted by mutations of three conserved aromatic residues (Y148, Y155 and W170) in the second PHD domain (Extended Data Fig. 8g–j). Another MAS subunit, SHH2, was previously reported to bind to H3K4me3 as determined by an *in vitro* assay<sup>50</sup>. The binding of histone acetylation and/or H3K4me3 by the BAS and MAS subunits is probably required for the occupancy of the BAS and MAS complexes on genes with high levels of histone acetylation and H3K4me3.

While the BAS complex has acetylated histone-binding subunits BRD1/2/13, the MAS complex contains both the acetylated histone-binding subunit BRD5 and the H3K4me3-binding subunits PMS2A/B and SHH2, which explains that the MAS-occupied genes are more active than the BAS-occupied genes. Unlike the BAS and MAS complexes, the SAS complex lacks any known readers of active histone modifications, which is associated with the fact that the SAS-occupied regions are more repressive than both the BAS- and MAS-occupied regions. Moreover, because H3ac and H3K4me3 are mainly located at the TSS-flanking intragenic region (Extended Data Fig. 7c), the recognition of histone acetylation and/or H3K4me3 by the MAS and BAS subunits provides a plausible explanation for the higher enrichment of the MAS and BAS complexes than of the SAS complex at the TSS-flanking intragenic region (Fig. 4b).

**BAS, SAS and MAS primarily enhance chromatin accessibility**  
To investigate whether the SWI/SNF complexes regulate chromatin accessibility, we performed assay for transposase-accessible chromatin followed by sequencing (ATAC-seq) for the BAS, SAS and MAS mutants and the wild type. On the basis of the principal component analysis of ATAC-seq data, the SWI/SNF mutants were divided into three groups that exactly corresponded to the three classes of SWI/SNF complexes (Fig. 5a), suggesting that the three classes of SWI/SNF complexes have specific functions in the regulation of chromatin accessibility. Analysis of the ATAC-seq data identified thousands of differentially accessible regions (DARs; false discovery rate <0.05,  $| \log_2(\text{fold change}) | \geq 0.5$ ) in the SWI/SNF mutants relative to the wild-type plants, with most of the DARs showing reduced rather than increased accessibility in all the tested SWI/SNF mutants (Extended Data Fig. 9a and Supplementary Data 6), indicating that the SWI/SNF complexes primarily enhance chromatin accessibility. We therefore focused mainly on those DARs with reduced accessibility in order to investigate how the SWI/SNF complexes enhance chromatin accessibility in the following analyses. To determine whether the SWI/SNF complexes directly enhance chromatin accessibility, we compared ChIP-seq and ATAC-seq data and found that most of the BAS-, SAS- or MAS-dependent accessible regions are bound by the corresponding types of SWI/SNF components (Extended Data Fig. 9b), supporting the direct effect of SWI/SNF complexes on chromatin accessibility.

We generated DAR-associated genes and pairwise compared them in different SWI/SNF mutants, indicating that the DAR-associated genes identified in the mutants of the same SWI/SNF complex are closely related to each other and are distantly related to those in the mutants of the other SWI/SNF complexes, suggesting that BAS-, SAS- and MAS-dependent accessibility occurs at different sets of genes (Fig. 5b, Extended Data Fig. 9c and Supplementary Data 6). Besides, there was a weak negative correlation between the accessibility of SAS and MAS mutants (Fig. 5b), indicating that the two complexes have an

antagonistic effect on chromatin accessibility at their common target genes. Gene Ontology (GO) analysis indicated that the genes with reduced accessibility in the BAS mutants and SAS mutants are especially enriched in the terms of development and stress response, while the genes with reduced accessibility in MAS mutants are enriched in the terms of biosynthetic and metabolic processes (Supplementary Data 7).

To investigate whether the BAS/SAS/MAS-dependent chromatin accessibility is related to histone modifications, we divided the SWI/SNF-bound regions into two groups on the basis of whether the chromatin accessibility is or is not downregulated in the corresponding SWI/SNF mutants, and then compared the levels of H3ac, H3K4me3 and H3K27me3 between the two groups. Reduced chromatin accessibility in *brm*, *syd* and *minu1/2* mutants were defined as BAS-, SAS- and MAS-dependent accessibility, respectively. We found that BAS/MAS-dependent accessibility is prone to occur at those BAS/MAS-bound regions with relatively high levels of active histone modifications, whereas SAS-dependent accessibility is prone to occur at those SAS-bound regions with relatively low levels of active histone modifications (Fig. 5c). In line with the higher levels of the active histone modifications in the BAS-dependent accessible regions than in the SAS-dependent accessible regions, the level of the repressive histone modification H3K27me3 was lower in the BAS-dependent accessible regions than in the SAS-dependent accessible regions (Extended Data Fig. 9d). These results suggest that the active histone modifications are positively related to the BAS/MAS-dependent chromatin accessibility and negatively related to the SAS-dependent accessibility.

### SWI/SNF-dependent accessibility at different genomic regions

While all accessible regions are enriched at the TSS-flanking regions, the distribution patterns of BAS-, SAS- and MAS-dependent accessible regions are different from the distribution pattern of all accessible regions (Fig. 5d). The SAS-dependent accessible regions are enriched at distal promoter regions (400–1,000 bp upstream of TSS) and intergenic regions, whereas the BAS- and MAS-dependent accessible regions are located mainly at proximal promoter regions (1–400 bp upstream of TSS) and 5' untranslated region (UTR) but are depleted at distal promoter regions or intergenic regions (Fig. 5d). By analysing the proportion of BAS-, SAS- and MAS-dependent accessible regions to all accessible regions annotated to each chromatin feature (Fig. 5e), we found that the SAS complex regulates ~40% of accessible regions at distal promoter or intergenic regions, which is substantially higher than those regulated by BAS and MAS (~10%). By drawing heat maps and metaplots for BAS-, SAS- and MAS-dependent accessible signals, we found that, while the BAS-, SAS- and MAS-dependent accessible signals formed a peak at the TSS-flanking region, the SAS-dependent accessible signals formed an additional peak at the distal promoter region (Fig. 5f and Extended Data Fig. 10a, b). These results suggest that, while all three classes of SWI/SNF complexes are involved in chromatin accessibility at TSS-flanking regions, SAS plays a major role in mediating chromatin accessibility at distal promoter regions and intergenic regions.

We then plotted the profiles of ChIP-seq signals for the BAS, SAS and MAS components at the BAS-, SAS- and MAS-dependent accessible genes. The ChIP-seq data indicated that all the tested BAS, SAS and MAS components formed a TSS-flanking peak at their target genes, and that the accessibility mediated by each SWI/SNF complex was associated with the highest enrichment of the corresponding SWI/SNF components (Fig. 5f,g); this indicated that the SWI/SNF complexes directly regulate chromatin accessibility at TSS-flanking regions. Moreover, the SAS components formed an additional peak at the SAS-regulated distal accessible regions (Fig. 5g), indicating that the SAS complex directly regulates the accessibility of distal regions. The BAS components also formed an additional peak at the SAS-regulated distal accessible regions, and the accessibility of these regions was weakly reduced in the BAS mutant (Fig. 5f and Extended Data Fig. 10a,b). These results suggest that the SAS complex and to a lesser extent the BAS complex directly

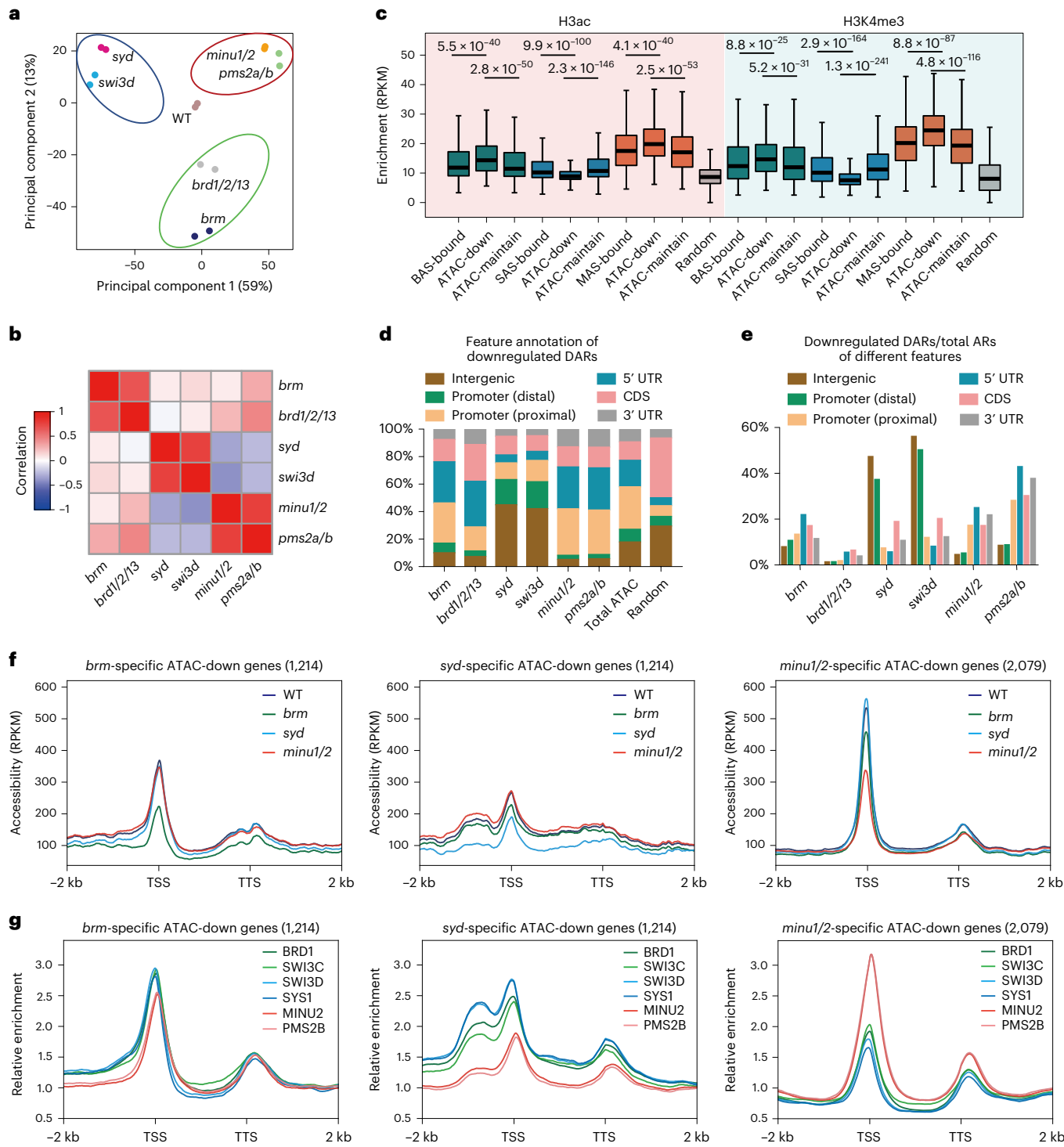


**Fig. 5 | Distinct effects on chromatin accessibility of BAS, SAS and MAS complexes.** **a**, Principal component analysis (PCA) of the indicated ATAC-seq samples. Percentages represent variance captured by PC1 and PC2 in each analysis. Clusters of BAS, SAS and MAS mutants are labelled by green, blue and red circles, respectively. WT, wild type. **b**, Heat map showing the pairwise Pearson correlation coefficient of the indicated SWI/SNF mutants based on  $\log_2(\text{mutant}/\text{WT})$  of ATAC peak reads at the total genes with changed accessibility in SWI/SNF mutants relative to the wild type. **c**, Box plots showing the H3ac and H3K4me3 levels of the regions bound by each complex and the regions bound by each complex with decreased or maintained accessibility. Random: 10,000 random genomic regions (1,000 bp). The sample size of each box plot: BAS-bound ( $n = 12,392$ ), ATAC-down ( $n = 1,470$ ), ATAC-maintain ( $n = 10,922$ ), SAS-bound ( $n = 11,398$ ), ATAC-down ( $n = 2,195$ ), ATAC-maintain ( $n = 9,203$ ), MAS-bound ( $n = 11,129$ ), ATAC-down ( $n = 1,637$ ), ATAC-maintain ( $n = 9,492$ ),

random ( $n = 10,000$ ). In box plots, centre lines and box edges are medians and the interquartile range (IQR), respectively. Whiskers extend within 1.5 times the IQR.  $P$  values were determined by two-tailed Mann–Whitney  $U$  test. **d**, The proportion of downregulated DARs annotated to a specified chromatin feature to total downregulated DARs in each indicated SWI/SNF mutant. Distal promoter: -400–1,000 bp upstream of the TSS. Proximal promoter: -1–400 bp upstream of the TSS. Total ATAC: ATAC peaks identified in the wild type. Random: 8,000 random genomic regions. **e**, The proportion of downregulated DARs in each SWI/SNF mutant to total accessible regions (ARs) annotated to a specified chromatin feature. **f,g**, Profile plots showing the accessibility signals in the indicated SWI/SNF mutants (**f**) and the ChIP enrichment signals of indicated SWI/SNF components (**g**) at genic regions with decreased accessibility specifically identified in *brm*, *syd* and *minu1/2*, respectively. WT, wild type. TSS, transcription start site; TTS, transcription termination site.

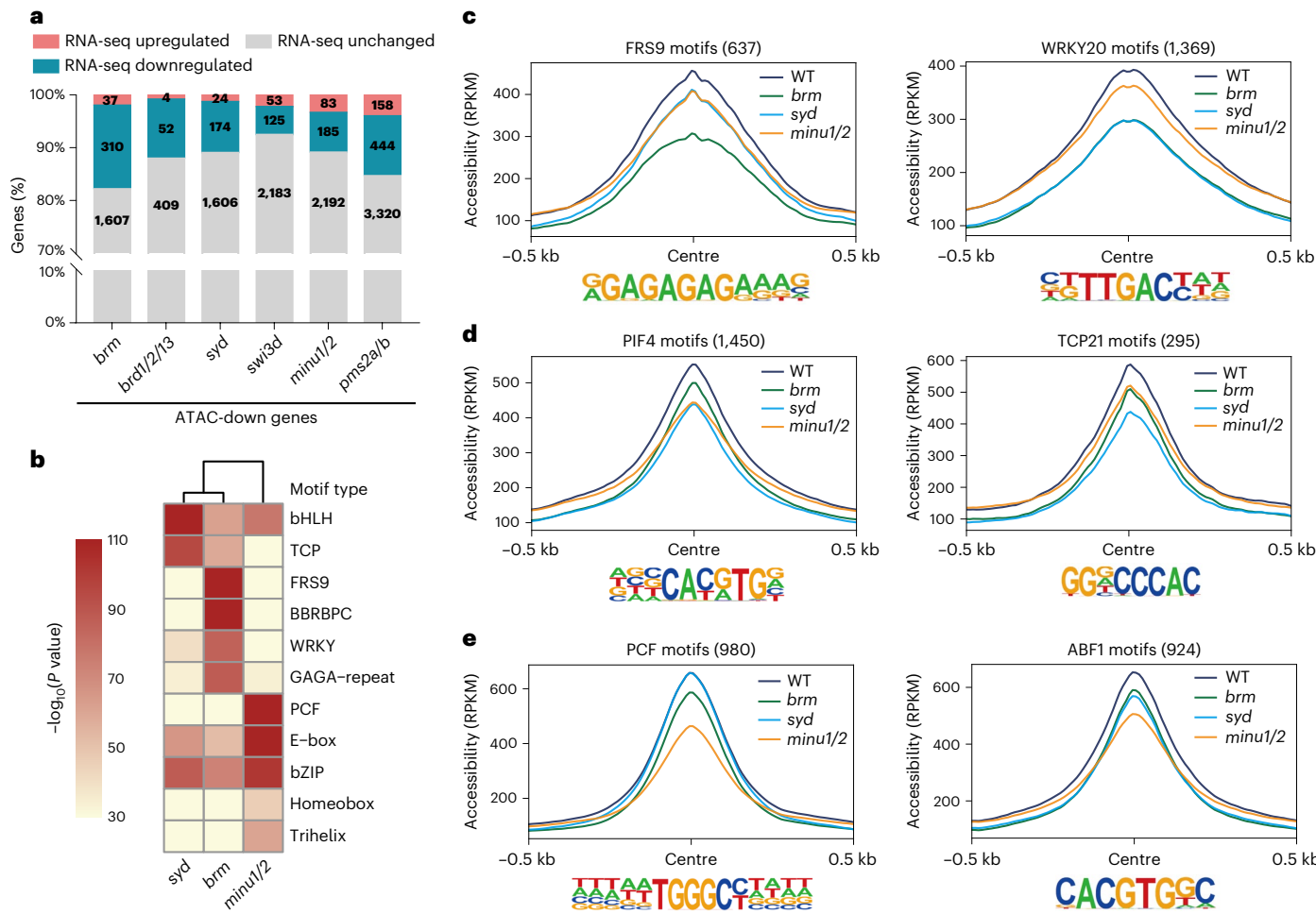


**Fig. 6 | Enrichment of different transcription-factor-binding motifs in the accessible regions maintained by BAS, SAS and MAS. a**, The percentage of genes with upregulated, downregulated and unchanged expression among genes with decreased accessibility in indicated mutants relative to the wild type. **b**, Heat map showing the enrichment levels of different motif types at the decreased accessible regions in *syd*, *brm* and *minu1/2*. **c–e**, Accessibility profiles of the flanking regions of indicated transcription-factor-binding motifs in wild type

and indicated mutants. Total regions with decreased accessibility in *brm*, *syd* and *minu1/2* were subjected to the analysis. The transcription-factor-binding motifs enriched at the decreased accessible regions in *brm* (**c**), *syd* (**d**) and *minu1/2* (**e**) are independently presented. In brackets, the number of motifs located in the total regions with decreased accessibilities in *brm*, *syd* and *minu1/2* is indicated. Reads are normalized by reads per kilobase per million mapped reads (RPKM). WT, wild type.

regulate chromatin accessibility at distal regions. In the MAS mutant, however, the chromatin accessibility was weakly increased rather than reduced at those SAS-dependent distal accessible regions (Fig. 5f and Extended Data Fig. 10b), which is consistent with the antagonistic effect of SAS and MAS mutations as indicated by the correlation analysis of ATAC-seq data (Fig. 5b). Further investigation is required to determine how MAS antagonizes SAS to regulate chromatin accessibility.

**Specific DNA motifs in SWI/SNF-dependent accessible regions**  
To determine whether SWI/SNF-dependent chromatin accessibility is associated with the regulation of gene expression, we compared the ATAC-seq and RNA-seq data and found that 10–20% of the genes with reduced accessibility are differentially expressed in the corresponding SWI/SNF mutants; among these DEGs, the number with reduced expression is consistently higher than the number with increased expression in each SWI/SNF mutant (Fig. 6a). These analyses indicate that the SWI/SNF-dependent accessible regions are primarily responsible for the activation of transcription.

To investigate whether specific transcription-factor-binding DNA motifs are related to SWI/SNF-dependent accessible regions, we used Hypergeometric Optimization of Motif EnRichment (HOMER)<sup>55</sup>

to perform a motif enrichment analysis. We found that the binding motifs of different transcription factor families are differently enriched at the BAS-, SAS- and MAS-dependent accessible regions. The WRKY family transcription-factor-binding motif is enriched more at BAS-dependent accessible regions; the TCP and bHLH family transcription-factor-binding motifs are enriched more at SAS-dependent accessible regions; and the PCF and bZIP family transcription-factor-binding motifs are enriched more at MAS-dependent accessible regions (Fig. 6b and Supplementary Data 8). Consistent with a previous report<sup>56</sup>, our analysis indicated that the binding motif of the light-regulated transcription factor FRS9 is enriched at the BAS-dependent accessible regions (Fig. 6b), indicating the reliability of the analysis.

By profiling the accessibility of SWI/SNF-dependent accessible regions centred by the transcription-factor-binding motif in wild type, *brm*, *syd* and *minu1/2*, we found that the accessibility signals form a peak at tested transcription-factor-binding motifs in SWI/SNF-dependent accessible regions (Fig. 6c–e), suggesting that SWI/SNF-dependent accessibility is related to the chromatin binding of these transcription factors. Moreover, we found that the accessibility signals are reduced to different extents in *brm*, *syd* and *minu1/2* relative

to the wild type (Fig. 6c–e). At the accessible regions centred by each transcription-factor-binding motif, the reduced accessibility levels in *brm*, *syd* and *minu1/2* mutants are generally consistent with the enrichment levels of the corresponding transcription-factor-binding motif (Fig. 6b–e), supporting the notion that accessible regions regulated by three classes of SWI/SNF complexes are related to different sets of transcription factors. The three classes of SWI/SNF complexes may mediate chromatin accessibility for different sets of transcription factors, thereby contributing to the specific functions of the BAS, SAS and MAS complexes in development.

## Discussion

In this study, we identified three classes of SWI/SNF complexes in *Arabidopsis* and rice and indicated the whole-genome profiles of the *Arabidopsis* SWI/SNF complexes. During the review of our manuscript, a recent study reported the identification of a MINU2-associated complex<sup>57</sup>, and the complex composition identified in that study is identical to the composition of the MAS complex identified in our study, confirming that the composition and classification of SWI/SNF complexes as determined by our study are convincing. Three classes of SWI/SNF complexes contain both subunits that are unique to one type of SWI/SNF complex and subunits that are shared by two or three types of SWI/SNF complex. We performed phenotypic analyses for the mutants of three types of SWI/SNF complex, and found that three classes of SWI/SNF complexes have both overlapping and specific functions in the regulation of development, which is consistent with previous phenotypic analyses<sup>8,10,17,33,43</sup>. The results shown in the current study indicated that three types of SWI/SNF complex differently regulate chromatin accessibility, providing a plausible explanation for the specific functions of different SWI/SNF complexes.

This study indicated that all the three classes of SWI/SNF complexes predominantly bind to the TSS-flanking regions of protein-coding genes, suggesting that the SWI/SNF complexes share certain intrinsic features that are responsible for binding to the TSS-flanking region. However, the distribution patterns of BAS, SAS and MAS are different at up- and downstream regions of the TSS. While the BAS complex mainly binds to the TSS-flanking region, the distribution of SAS and MAS extends from the TSS-flanking region to the upstream distal region and the downstream intragenic region, respectively (Figs. 4b and 7). Considering that the active histone modifications H3ac and H3K4me3 are mainly enriched at the intragenic region<sup>25,45,48</sup>, we suspect that the different distribution patterns of BAS, SAS and MAS are caused by the different binding abilities of BAS, SAS and MAS for active histone modifications. As determined by this study and a previous study<sup>50</sup>, the MAS complex contains one histone acetylation reader (BRD5) and two H3K4me3 readers (SHH2 and PMS2A/B). These active histone modification readers may enable the binding of MAS to the intragenic region (Fig. 7). The BAS complex contains only one conserved histone acetylation reader that is encoded by three homologous genes (*BRD1*, *BRD2* and *BRD13*) and is likely to have a weaker binding ability for active histone modifications than the MAS complex. Thus, the BAS complex binds to the intragenic region to a lesser extent than the MAS complex (Fig. 7). Unlike BAS and MAS, the SAS complex lacks any known readers of active histone modifications, which is consistent with the finding that the SAS-bound region extends from the TSS-flanking region to the up-stream distal region with low levels of active histone modifications (Fig. 7). These analyses suggest that the different binding abilities of BAS, SAS and MAS for active histone modifications are probably responsible for their binding to different regions of target genes.

Moreover, we found that the active histone modifications are also likely to differently affect the function of BAS, SAS and MAS in mediating chromatin accessibility. The BAS/MAS complexes are prone to mediate chromatin accessibility at the intragenic region with high levels of active histone modifications, whereas the SAS complex is prone to mediate chromatin accessibility at the distal region with low

levels of active histone modifications (Figs. 4b, 5d and 7). Therefore, the active histone modifications regulate the function of BAS, SAS and MAS at both chromatin-binding level and the nucleosome remodelling level, although the underlying molecular mechanism remains elusive. In yeast and human, histone modifications have been demonstrated to affect the nucleosome remodelling activities of SWI/SNF complexes by biochemical analyses<sup>58,59</sup>. We infer that the recognition of histone modifications by specific modified-histone readers in SWI/SNF complexes is probably responsible for determining how the nucleosome remodelling activities of three classes of SWI/SNF complexes are differentially regulated.

Three human SWI/SNF complexes (BAF, PBAF and ncBAF) have been identified<sup>3</sup>. By comparing the compositions of SWI/SNF complexes between *Arabidopsis* and human, we found that the *Arabidopsis* Snf5 homologue BSH is a subunit of MAS but not of BAS or SAS. It is notable that the Snf5 homologue is also absent in the non-canonical BAF type of SWI/SNF chromatin remodelling complex (ncBAF) in human, implicating the Snf5 homologue is unlikely to be an essential component of all SWI/SNF complexes. In addition to the absence of the Snf5 homologue, the *Arabidopsis* BAS complex and the human ncBAF complex also share other features. The *Arabidopsis* BAS specific subunits BRIP1/BRIP2 are homologous to the human ncBAF specific subunits GLTSCR1/GLTSCR1L; the *Arabidopsis* LFR and its human homologue BAF200/250 are absent in the *Arabidopsis* BAS complex and the human ncBAF complex, respectively, but not in any other human or *Arabidopsis* SWI/SNF complexes. These analyses indicate that the *Arabidopsis* BAS complex is an analogue of the human ncBAF complex. Although the MAS complex contains a short SWI/SNF ATPase version that is unique in plants, several specific subunits of MAS (BSH, BRD5 and PMS1A/1B/2A/2B) are homologous to subunits of the human PBAF complex. In human, the PBAF complex that is predominantly responsible for chromatin accessibility at promoter regions rather than at distal enhancer regions<sup>60,61</sup>. In *Arabidopsis*, whole-genome analyses have identified accessible loci both at promoter regions and distal regions<sup>62</sup>. We found that the MAS-dependent accessibility occurs primarily at TSS-flanking proximal promoter regions. These analyses support the inference that the *Arabidopsis* MAS complex is a counterpart of the human PBAF complex.

This study indicated that the SAS complex is a major SWI/SNF complex that is responsible for mediating chromatin accessibility at distal promoter regions and intergenic regions. As active histone modifications are absent at the distal promoter and intergenic regions, it is reasonable to find the SAS-dependent accessibility prone to occur at relatively low levels of active histone modifications. In human, the accessibility of distal enhancer regions and bivalent promoter regions is mainly regulated by the BAF-type SWI/SNF complex<sup>60,61</sup>. It follows that the *Arabidopsis* SAS complex is likely to be a functional analogue of the human BAF complex. However, unlike the SAS complex, which lacks a subunit that functions as a reader of histone acetylation or methylation, the BAF complex not only contains a bromodomain-containing ATPase (BRM or BRG1) that recognizes histone acetylation but also contains three redundant accessory subunits (DPF1, DPF2 and DPF3) that function as readers of histone acetylation and H3K4 methylation<sup>63,64</sup>. In particular, DPF3 binds to H3K4me1, a hallmark of active enhancers, and is required for the association of the BAF complex with chromatin<sup>65</sup>. Given that the histone modifications H3K4me1 and H3K27ac are enriched at distal accessible regions in mammals but not in plants<sup>65,66</sup>, the lack of a reader of the histone modifications in the SAS complex is likely to represent a plant-specific property that is related to the lack of the histone modifications in distal accessible regions. The interplay between the composition of SWI/SNF complexes and the histone modification pattern indicates that the SWI/SNF complexes have evolved a flexible selection of different histone readers and a fine-tuned adaptation to transcriptional regulation in *Arabidopsis*. Considering the conserved types of SWI/SNF ATPases in plants and

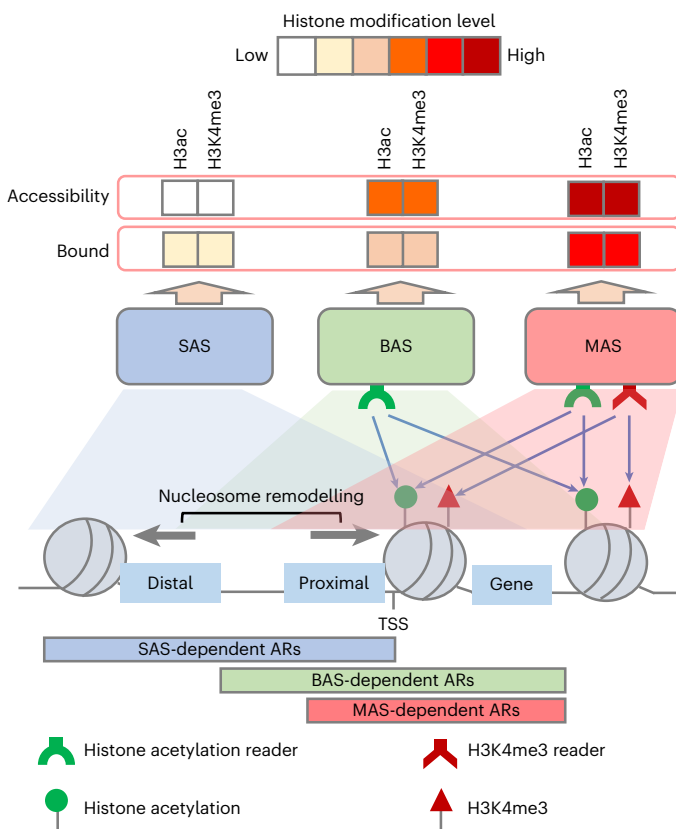


**Fig. 7 | Different effects of SAS, BAS and MAS complexes on chromatin accessibility at TSS-flanking regions.** The SAS-, BAS- and MAS-bound regions are indicated by blue, green and red shadows, respectively. Colour boxes shown on the top represent histone modification levels of SWI/SNF-bound regions and of SWI/SNF-dependent accessibility regions (ARs). Blue, green and red bars shown at the bottom represent the locations of major SAS-, BAS- and MAS-dependent accessible regions, respectively. BAS complex contains a histone acetylation reader (BRD1/BRD2/BRD13); the MAS complex contains both a histone acetylation reader (BRD5) and two H3K4me3 readers (PMS2A/PMS2B and SHH2); the SAS complex lacks a reader of the active histone modifications (histone acetylation or H3K4me3).

the conserved composition of the three classes of SWI/SNF complexes in *Arabidopsis* and rice, our research provides a basic understanding of the composition and function of SWI/SNF complexes that is widely applicable in plants.

Although histone modification readers are responsible for the association of SWI/SNF complexes with specific chromatin regions, the targeting of SWI/SNF complexes may require pioneer transcription factors, which initially bind to nucleosomal DNA and then recruit the SWI/SNF complexes to chromatin in order to mediate chromatin accessibility for additional transcription factors<sup>67</sup>. In *Arabidopsis*, the critical floral identity regulators AP1, SEP3 and LFY were reported to function as pioneer transcription factors in order to regulate floral development<sup>68,69</sup>. Moreover, several transcription factors have been shown to interact with one or more SWI/SNF components and to then regulate the expression of genes involved in multiple biological processes<sup>12,41,70–73</sup>, although whether these SWI/SNF-interacting transcription factors are pioneer transcription factors or not remains unknown. Considering that chromatin accessibility is dynamically regulated during various developmental processes<sup>56,74–77</sup>, it is important to investigate how the three classes of SWI/SNF complexes coordinate with different transcription factors to regulate specific developmental processes. The finding of the locus-specific binding and nucleosome remodelling

abilities of the three classes of SWI/SNF complexes in the current study provides a framework for investigating the coordination of the SWI/SNF complexes with transcription factors. Further studies are required to elucidate how the three classes of SWI/SNF complexes coordinate with various transcription factors to regulate development.

## Methods

### Plant materials

*Arabidopsis* materials used in this study were in the Columbia-0 (Col-0) ecotype. The following *Arabidopsis* T-DNA insertion mutants were obtained from the *Arabidopsis* Biological Resource Center or the Nottingham *Arabidopsis* Stock Center: *brm-1* (SALK\_030046C), *brd1* (GK-219B04, SALK\_012963), *brd2* (SALK\_025965), *brd13* (SALK\_208635), *brip1* (SALK\_133464), *brip2* (SALK\_117513), *syd* (CS822017), *swi3d* (SALK\_100310), *minu1* (SALK\_015562), *minu2* (SALK\_057856), *pms2a* (SALK\_141512), *pms2b* (SALK\_010411), *swp73b* (SALK\_113834), *bcl7a* (SALK\_027934), *bcl7b* (SALK\_029285) and *an3* (SALK\_150407). The double mutants *brip1/2*, *minu1/2*, *pms2a/2b* and *bcl7a/b*, and the triple mutant *brd1/2/13* were generated by crossing. The triple mutant *syd1/2/3* was generated using the clustered regularly interspaced short palindromic repeats (CRISPR)–Cas9 system according to previously reported methods<sup>78</sup>. The genotyping primers are listed in Supplementary Data 9.

Full-length genomic sequences of genes without stop codons driven by a 1.5–2.0 kb native promoter were cloned into modified pCAMBIA1305-Flag to generate C-terminal 3× Flag-tagged transgenes. In this way, *SWP73A*, *SWP73B*, *BCL7A*, *BCL7B*, *ARP4*, *ARP7*, *SWI3C*, *BRD1*, *BRD2*, *BRD13*, *BRIP1*, *BRIP2*, *AN3*, *GIF2*, *SWI3D*, *SYS1*, *LFR*, *MINU2*, *SWI3A*, *SWI3B*, *BSH*, *SHH2*, *PMS1A*, *PMS2A* and *PMS2B*, and the genomic sequences encoding SYDAC and SYD-C proteins were cloned into pCAMBIA1305-Flag. The full-length coding sequence of *BRM* driven by its native promoter was cloned into pCAMBIA1305-Flag. *BRD1*, *SYDAC*, *SWI3C*, *SWI3D*, *SYS1*, *MINU2* and *PMS2B* were also cloned into modified pCAMBIA1305-GFP to generate C-terminal GFP-tagged transgenes. The constructs were introduced into *Agrobacterium tumefaciens* strain GV3101 and were transformed into wild-type or mutant plants using the floral dip method. For transgenic rice, the full-length coding sequence (CDS) region of *OsBCL7*, *OsBRIP*, *OsCHB704*, *OsLFR* and *OsBSH* were amplified from rice complementary DNA and cloned into pMDC43 to generate N-terminal GFP-tagged transgenes driven by a 35S promoter. The constructs were introduced into *A. tumefaciens* strain EHA105. Transformation of rice was performed by the Biogate Corporation as previously described<sup>79</sup>. Primers for the transgene constructs are listed in Supplementary Data 9.

### Growth conditions

After *Arabidopsis* seeds were sown on Murashige and Skoog medium and stratified at 4 °C for 2 days, they were grown under long-day conditions (16 h of light at 23 °C and 8 h of darkness at 22 °C). Twelve-day-old seedlings were used for AP-MS, RNA-seq, ATAC-seq and ChIP experiments. Eight-day-old seedlings were transferred to soil and grown under the same conditions for genotyping, phenotype analysis and harvesting of inflorescence tissues. Rice seeds were soaked in water at room temperature for 2 days and then kept at 37 °C on wet gauze until they germinated. The germinated seeds were transferred to soil and cultivated at 28 °C (16 h of light and 8 h of darkness).

### AP-MS

Plant materials for affinity purification were harvested and ground in liquid nitrogen. For *Arabidopsis*, about 2 g of 12-day-old seedlings and 2 g of inflorescence tissues were used. For rice, about 4 g of young leaf tissue was used. The fine powder was suspended in 15 ml of ice-cold lysis buffer (50 mM Tris-HCl at pH 7.6, 150 mM NaCl, 5 mM MgCl<sub>2</sub>, 10% glycerol, 0.1% NP-40, 0.5 mM dithiothreitol (DTT), 1 mM PMSF and one tablet of Roche protease inhibitor cocktail per 50 ml) and incubated for 15 min at 4 °C, followed by centrifugation at 12,000g for 15 min. The

supernatant was passed through two layers of Miracloth and incubated with anti-Flag M2 Affinity Gel (A2220; Sigma-Aldrich) at 1:200 dilution (for *Arabidopsis*) or agarose beads (Cytiva, 1709601) coupled with GFP-binding protein (GBP) (for rice) at 1:100 dilution for 2.5 h at 4 °C. The agarose beads were centrifuged and washed four times with lysis buffer to remove the non-specific binding proteins. 3× Flag peptides (Sigma, F4799) were added to elute the binding proteins. The eluate was separated on a 10% SDS-PAGE gel followed by silver staining with the ProteoSilver Silver Stain Kit (Sigma, PROT-SIL1).

Mass spectrometry analysis was performed as previously described<sup>50</sup>. In brief, the silver-stained gels were excised, de-stained and subjected to in-gel digestion with trypsin overnight at 37 °C; the peptides were then eluted on a capillary column and sprayed into a Q Exactive Mass Spectrometer equipped with a nano-ESI ion source (Thermo Fisher Scientific). The acquired spectra were searched in the International Protein Index database for *Arabidopsis* and in the National Center for Biotechnology Information (NCBI) database for rice on the Mascot server (Matrix Science, version 2.6.0). Microsoft Excel (Office 365) and GraphPad Prism (version 7) software was used to generate the heat map of normalized matched queries detected by AP-MS.

### Y2H assay

The full-length coding sequence and several truncated derivatives of *SWP73A*, *SWP73B*, *BCL7A*, *BCL7B*, *ARP4*, *ARP7*, *BRM*, *SWI3C*, *BRD1*, *BRD2*, *BRD13*, *BRIP1*, *BRIP2*, *AN3*, *GIF2*, *GIF3*, *SYD*, *SWI3D*, *SYS1*, *SYS2*, *SYS3*, *LFR*, *MINU2*, *SWI3A*, *SWI3B*, *BSH*, *SHH2*, *PMS1A*, *PMS1B*, *PMS2A*, *PMS2B*, *MIS* and *SSM* were cloned into pGADT7 (with GAL4-AD) and/or pGBTKT7 (with GAL4-BD) vectors using a One-Step Cloning Kit (Vazyme Biotech; C112). Primers used for Y2H constructs are listed in Supplementary Data 9. The yeast strains AH109 and Y187 were transformed with the GAL4-AD and GAL4-BD constructs, respectively. The strain AH109 was grown on synthetic dropout medium lacking Leu (SD-L), and the strain Y187 was grown on synthetic dropout medium lacking Trp (SD-W). After the colonies on SD-L and SD-W media were mated for 16–20 h in YPDA liquid culture medium, the mixture was spread on SD medium lacking Trp and Leu (SD-WL). Colonies on SD-WL were suspended in sterile ddH<sub>2</sub>O and spotted on SD medium lacking Trp, Leu and His (SD-WLH) but supplemented with 0, 1, 3 or 6 mM 3-amino-1,2,4-triazol.

### RNA isolation and RNA-seq analysis

TRIzol reagent (Invitrogen, 15596018) was used to extract total RNA from about 0.08 g of 12-day-old seedlings grown on Murashige and Skoog medium plates. Total RNA was sent to BGI (Wuhan, China) for library preparation and sequencing using the DNBSEQ platform (sequencing method: SE50). The presented data were obtained from three independent biological replicates. After removal of adapters and low-quality reads, the clean reads were aligned to the *Arabidopsis* genome (TAIR10) using HISAT2 (version 2.1.0) with the default parameters<sup>80</sup>. The reads mapped on the exon were counted using featureCounts (version 2.0.0) (ref. <sup>81</sup>). DEGs were identified with  $|\log_2 \text{FC}| \geq 1$  and  $\text{FDR} < 0.05$  using edgeR (version 3.28.1) (ref. <sup>82</sup>). To explore expression differences between the samples, MDS plot was generated by the plotMDS function of edgeR with default parameters. The heat map of DEGs was drawn using the R package Pheatmap (version 1.0.12) (ref. <sup>83</sup>). A heat map based on Pearson correlation coefficients was drawn using the heatmap.2 function of the R package gplots (version 3.0.3) (ref. <sup>84</sup>).

### ChIP-seq analysis

GFP-tagged transgenic plants were used for ChIP experiments, and wild-type Col-0 plants were used as the negative control. ChIP experiments were performed as previously described<sup>85</sup>. In brief, 4 g of 12-day-old seedlings grown on Murashige and Skoog medium were harvested and crosslinked with 1% formaldehyde for 12 min under vacuum. The plant materials were then ground into fine powder in liquid nitrogen and suspended in NEB I (10 mM Tris-HCl at pH 8.0,

0.4 M sucrose, 10 mM MgCl<sub>2</sub>, 0.1 mM DTT, 1 mM PMSF and one tablet of Roche protease inhibitor cocktail per 50 ml) at 4 °C. After filtering, the nuclei were centrifuged and washed by NEB II (10 mM Tris-HCl at pH 8.0, 0.25 M sucrose, 10 mM MgCl<sub>2</sub>, 1% Triton X100, 0.1 mM DTT, 1 mM PMSF and one tablet of Roche protease inhibitor cocktail per 50 ml). The nuclei were then resuspended in NEB III (10 mM Tris-HCl at pH 8.0, 1.7 M sucrose, 2 mM MgCl<sub>2</sub>, 0.15% Triton X100, 0.1 mM DTT and 1 mM PMSF) and overlaid onto NEB III with the same volume, followed by centrifugation at 16,000g for 1 h at 4 °C. Chromatin was extracted, fragmented using the Bioruptor sonicator, and incubated with GFP antibody (Abcam, ab290, 1:600 dilution) coupled with Dynabeads Protein A (Invitrogen, 100.01D) at 4 °C overnight. The beads were successively washed with low-salt washing buffer, high-salt washing buffer, LiCl buffer and TE buffer. The binding protein-DNA complexes were then eluted and subsequently subjected to reverse crosslinking, RNase digestion and proteinase K digestion. Immunoprecipitated DNA was purified for library construction followed by high-throughput sequencing.

ChIP-seq libraries were constructed using the NEBNext Ultra DNA Library Prep Kit for Illumina (NEB) by Novogene. High-throughput sequencing was performed using Illumina-NovaSeq (sequencing method: PE150). For ChIP-seq analysis, adapters and low-quality reads were removed, and the clean reads were mapped to the *Arabidopsis* genome (TAIR10) by bowtie2 (version 2.3.5.1). MACS2 (version 2.2.7.1) (ref. <sup>86</sup>) was used for peak calling using the following parameters: ‘-f BAMPE -g 119145879 -bdg -nomodel’. For further analysis, only the peaks that were present in both replicates (irreproducible discovery rate  $\leq 0.05$ ) were considered. A peak that overlapped with the gene body including 1 kb upstream was assigned to the corresponding gene. If a peak overlapped with two genes, it was annotated to the gene whose TSS was closest to the peak. To visualize the sequencing data, the unique mapped reads were converted to bigwig files using bamCoverage with ‘-binSize 10’ and ‘-normalizeUsing RPKM’ in DeepTools (version 3.4.3) (ref. <sup>87</sup>). ChIP-seq signals were visualized by JBrowse (<https://github.com/GMOD>). The heat map and box plots were drawn using the plotHeatmap of deepTools (version 3.4.3) and the box plot function in R (version 4.1.0), respectively.

### Protein expression and purification

The truncated sequences encoding the bromodomains of BRD1, BRD2 and BRD13 as well as the mutated bromodomain of BRD1 were cloned into the modified *pET28a* vector to generate N-terminal HIS-tagged proteins. The truncated sequences encoding the PHD domains of PMS1A and PMS2B as well as the mutated PHD domains of PMS2B were cloned into the *pGEX6P-1* vector to generate N-terminal GST-tagged proteins. The primers used for protein purification constructs are listed in Supplementary Data 9. The constructs were transformed into *Escherichia coli* strain BL21 (Rosetta DE3), and the bacteria were cultivated at 37 °C until the OD<sub>600</sub> values reached 0.8. The fused proteins were induced with 0.1 mM IPTG at 16 °C for 16 h. The bacterial cells were precipitated and then suspended in His-tag lysis buffer (20 mM Tris-HCl at pH 8.0, 500 mM NaCl, 20 mM imidazole, 1 mM DTT and 1 mM PMSF) or GST-tag lysis buffer (20 mM Tris-HCl at pH 7.6, 500 mM NaCl, 1 mM DTT and 1 mM PMSF), followed by sonication and centrifugation at 18,000g for 1 h at 4 °C. The supernatant was incubated with Ni-NTA HisBind Resin (Millipore, 70666-4) for HIS-tagged protein or with Glutathione Sepharose 4B (Cytiva, 10305042) for GST-tagged protein, and the bound proteins were eluted with His-tag elution buffer containing 250 mM imidazole or the GST-tag elution buffer containing 20 mM GSH. Purified proteins were separated on an SDS-PAGE gel followed by Coomassie blue staining to verify their molecular weight and purity.

### ITC assay

The purified proteins were concentrated and exchanged into ITC buffer (20 mM Tris-HCl at pH 7.5 and 100 mM NaCl) using Amicon

Ultra Centrifugal Filters (Millipore, UFC901096) at 4 °C; the proteins were then diluted to 0.05 mM with the ITC buffer. Histone peptides were dissolved in the same buffer and adjusted to 0.75 mM. The ITC binding assay was performed using a MicroCal PEAQ-ITC instrument (Malvern) at 25 °C. Binding was performed using the standard protocol, and the data were fit using the Origin 7.0 program (<https://www.originlab.com>). Histone peptides used in this assay were unmodified H3(1-19); H3(1-19)K4,9,14,18ac; unmodified H4(1-20); and H4(1-20)K5,8,12,16ac. All peptides were synthesized by SciLight Peptide.

### In vitro peptide pull-down assay

A 1 µg quantity of biotinylated histone peptides and 5 µg of purified GST-tagged proteins were added together to a 1.5 ml tube containing 300 µl of cold binding buffer (50 mM Tris-HCl at pH 7.5, 150 mM NaCl and 0.05% NP-40). A tube without peptides served as the no-peptide negative control. A 0.1 µg quantity of the protein was used as the 10% input. After the mixture was rotated slowly for 4 h at 4 °C, 25 µl of Streptavidin MagneSphere Paramagnetic Particles (Promega, Z5481) was added to each tube and incubated at 4 °C for 2 h. The beads were washed four times with 1 ml of cold binding buffer and were resuspended in 40 µl of 1× SDS loading buffer. The proteins bound by the beads and the input sample were boiled at 98 °C for 10 min and subjected to SDS-PAGE for western blot. GST antibody (Abmart, M20007L) diluted at 1:5,000 was used to detect the GST-tagged protein. Histone peptides used in this assay were H3(1-19) unmodified, H3(1-21) K4me1, H3(1-21)K4me2, H3(1-21)K4me3, H3(1-21)K9me1, H3(1-21) K9me2, H3(1-21)K9me3, H3(26-44)-unmodified, H3(26-44)K27me1, H3(26-44)K27me2, H3(26-44)K27me3, H3(26-44)K36me1, H3(26-44) K36me2 and H3(26-44)K36me3. All these peptides were synthesized by SciLight Peptide.

### ATAC-seq

About 0.1 g of 12-day-old seedlings grown on Murashige and Skoog medium were chopped into pieces in cold nuclei extraction buffer (10 mM Tris-HCl at pH 8.0, 0.25 M sucrose, 10 mM MgCl<sub>2</sub>, 0.3% Triton X100 and one tablet of Roche protease inhibitor cocktail per 50 ml). The slurry was then passed through a 40 µm cell strainer. Nuclei were collected by centrifugation at 1,000g for 10 min at 4 °C and were washed once with nuclei extraction buffer. After centrifugation, the nuclei were resuspended in nuclei purification buffer (20 mM MOPS at pH 7.0, 40 mM NaCl, 90 mM KCl, 2 mM EDTA, 0.5 mM EGTA, 0.5 mM spermidine, 0.2 mM spermine and one tablet of Roche protease inhibitor cocktail per 50 ml) and were examined with a microscope to verify their quality. About 10,000 to 50,000 nuclei were used for Tn5 fragmentation and library construction using the TruePrep DNA library Prep Kit V2 for Illumina (Vazyme, TD501). High-throughput sequencing was performed using an Illumina-NovaSeq 6000 at Novogene (sequencing method: PE150).

For ATAC-seq analysis, adapters and low-quality reads were removed by Trim Galore (version 0.6.6), and the trimmed reads were mapped to the *Arabidopsis* genome (TAIR10) by bowtie2 (version 2.3.5.1). Peak calling was done by MACS2 (version 2.2.7.1) with the following parameters: -f BAMPE -g 1.2e + 8-nomodel -bdg -keep-dup all. The ATAC-seq peaks were filtered, annotated and visualized with the same methods used in the ChIP-seq analysis. Principal component analysis and differential peak analysis were conducted by DiffBind (version 2.16.0) (ref. <sup>88</sup>). The heat map with Pearson correlation coefficients was drawn using the heatmap.2 function of the R package gplots (version 3.0.3) (ref. <sup>84</sup>). The profile plot and heat map were drawn using the plotProfile and plotHeatmap function of DeepTools (version 3.5.1) (ref. <sup>87</sup>). Box plots were drawn with the box plot function in R (version 4.1.0). GO analysis was done using clusterProfiler (version 3.16.1) (refs. <sup>89</sup>). Motif analysis was done using the findMotifsGenome.pl and scanMotifGenomeWide.pl program with default parameters in Homer (version 4.11.1) (ref. <sup>55</sup>).

### Domain prediction, sequence alignment and phylogenetic analysis

Protein sequences were downloaded from the TAIR, Uniprot and NCBI protein databases. The domains of each protein were predicted using NCBI conserved domain (CD)-Search tools. The schematic diagrams depicting the domain architecture were drawn using IBS-online (<http://ibs.biocuckoo.org/online.php>)<sup>90</sup>. Multiple sequence alignment and the homology tree generation were done by DNAMAN (version 8) software using default parameters or with slight adjustment. For phylogenetic analysis, the core protein sequences were aligned using the MUSCLE algorithm, and the phylogenetic tree was generated by MEGA (version 7) (ref. <sup>91</sup>) using the neighbour-joining method. Bootstrapping was performed with 500 replications.

### Reporting summary

Further information on research design is available in the Nature Portfolio Reporting Summary linked to this article.

### Data availability

A reporting summary for this paper is available as a Supplementary Information file. Raw data of RNA-seq, ChIP-seq and ATAC-seq results have been deposited in GEO (accession number [GSE193397](https://www.ncbi.nlm.nih.gov/geo/query/acc.cgi?acc=GSE193397)). The accession numbers of genes reported in this study are as follows: AT3G01890 (*SWP73A*), AT5G14170 (*SWP73B*), AT4G22320 (*BCL7A*), AT5G55210 (*BCL7B*), AT1G18450 (*ARP4*), AT3G60830 (*ARP7*), AT2G46020 (*BRM*), AT1G21700 (*SWI3C*), AT1G20670 (*BRD1*), AT1G76380 (*BRD2*), AT5G55040 (*BRD13*), AT3G03460 (*BRIP1*), AT5G17510 (*BRIP2*), AT5G28640 (*AN3*), AT1G01160 (*GIF2*), AT4G00850 (*GIF3*), AT2G28290 (*SYD*), AT4G34430 (*SWI3D*), AT5G07940 (*SYS1*), AT5G07970 (*SYS2*), AT5G07980 (*SYS3*), AT3G22990 (*LFR*), AT3G06010 (*MINU1*), AT5G19310 (*MINU2*), AT2G47620 (*SWI3A*), AT2G33610 (*SWI3B*), AT3G17590 (*BSH*), AT3G18380 (*SHH2*), AT1G50620 (*PMS1A*), AT3G20280 (*PMS1B*), AT3G08020 (*PMS2A*), AT3G52100 (*PMS2B*), AT1G58025 (*BRDS*), AT1G32730 (*MIS*), AT1G06500 (*SSM*), Os09g0284300 (*OsBCL7*), Os08g0137200 (*OsARP4*), Os03g0783000 (*OsARP7*), Os04g0382100 (*OsSWIB*), Os02g0114033 (*OsCHR707*), Os11g0183700 (*OsSWI3C*), Os12g0176700 (*OsCHB701*), Os03g0130800 (*OsBRD1*), Os09g0550000 (*OsBRD2*), Os12g0465700 (*OsDEC*), Os03g0733600 (*OsGIF1*), Os11g0615200 (*OsGIF2*), Os12g0496900 (*OsGIF3*), Os06g0255200 (*OsCHR720*), Os04g0110300 (*OsCHB704*), Os03g0213300 (*OssYS*), Os07g0609766 (*OsLFR*), Os05g0144300 (*OsCHR719*), Os04g0480300 (*OsCHB703*), Os02g0194000 (*OsCHB702*), Os02g0723700 (*OsBSH*), Os06g0485100 (*OsSHH2*), Os06g0309000 (*OsPMS1*), Os12g0527800 (*OsPMS2*), Os08g0109500 (*OsBRD5*), Os08g0129500 (*OsMIS*) and Os01g0246500 (*OsSSM*). Source data are provided with this paper.

### References

1. Clapier, C. R., Iwasa, J., Cairns, B. R. & Peterson, C. L. Mechanisms of action and regulation of ATP-dependent chromatin-remodelling complexes. *Nat. Rev. Mol. Cell Biol.* **18**, 407–422 (2017).
2. Hodges, C., Kirkland, J. G. & Crabtree, G. R. The many roles of BAF (mSWI/SNF) and PBAF complexes in cancer. *Cold Spring Harb. Perspect. Med.* **6**, a026930 (2016).
3. Michel, B. C. et al. A non-canonical SWI/SNF complex is a synthetic lethal target in cancers driven by BAF complex perturbation. *Nat. Cell Biol.* **20**, 1410–1420 (2018).
4. Mashitalir, N. et al. Modular organization and assembly of SWI/SNF family chromatin remodeling complexes. *Cell* **175**, 1272–1288 (2018).
5. Verbsky, M. L. & Richards, E. J. Chromatin remodeling in plants. *Curr. Opin. Plant Biol.* **4**, 494–500 (2001).
6. Han, S.-K., Wu, M.-F., Cui, S. & Wagner, D. Roles and activities of chromatin remodeling ATPases in plants. *Plant J.* **83**, 62–77 (2015).

7. Jerzmanowski, A. SWI/SNF chromatin remodeling and linker histones in plants. *Biochim. Biophys. Acta Gene Struct. Expr.* **1769**, 330–345 (2007).
8. Farrona, S., Hurtado, L., Bowman, J. L. & Reyes, J. C. The *Arabidopsis thaliana* SNF2 homolog AtBRM controls shoot development and flowering. *Development* **131**, 4965–4975 (2004).
9. Kwon, C. S. et al. A role for chromatin remodeling in regulation of CUC gene expression in the *Arabidopsis* cotyledon boundary. *Development* **133**, 3223–3230 (2006).
10. Wagner, D. & Meyerowitz, E. M. SPLAYED, a novel SWI/SNF ATPase homolog, controls reproductive development in *Arabidopsis*. *Curr. Biol.* **12**, 85–94 (2002).
11. Kwon, C. S., Chen, C. B. & Wagner, D. WUSCHEL is a primary target for transcriptional regulation by SPLAYED in dynamic control of stem cell fate in *Arabidopsis*. *Genes Dev.* **19**, 992–1003 (2005).
12. Li, C. et al. Concerted genomic targeting of H3K27 demethylase REF6 and chromatin-remodeling ATPase BRM in *Arabidopsis*. *Nat. Genet.* **48**, 687–693 (2016).
13. Shu, J. et al. Genome-wide occupancy of *Arabidopsis* SWI/SNF chromatin remodeler SPLAYED provides insights into its interplay with its close homolog BRAHMA and Polycomb proteins. *Plant J.* **106**, 200–213 (2021).
14. Bezhani, S. et al. Unique, shared, and redundant roles for the *Arabidopsis* SWI/SNF chromatin remodeling ATPases BRAHMA and SPLAYED. *Plant Cell* **19**, 403–416 (2007).
15. Mlynarova, L., Nap, J.-P. & Bisseling, T. The SWI/SNF chromatin-remodeling gene AtCHR12 mediates temporary growth arrest in *Arabidopsis thaliana* upon perceiving environmental stress. *Plant J.* **51**, 874–885 (2007).
16. Li, C., Zhao, J., Gao, Y. & Cui, S. Two putative chromatin-remodeling ATPases play redundant roles in seed and embryo development of *Arabidopsis*. *Plant Physiol.* **J.** **48**, 1084–1090 (2012).
17. Sang, Y. et al. Mutations in two non-canonical *Arabidopsis* SWI2/SNF2 chromatin remodeling ATPases cause embryogenesis and stem cell maintenance defects. *Plant J.* **72**, 1000–1014 (2012).
18. Brzeski, J., Podstolski, W., Olczak, K. & Jerzmanowski, A. Identification and analysis of the *Arabidopsis thaliana* BSH gene, a member of the SNF5 gene family. *Nucleic Acids Res.* **27**, 2393–2399 (1999).
19. Sarnowski, T. J., Swiezewski, S., Pawlikowska, K., Kaczanowski, S. & Jerzmanowski, A. AtSWI3B, an *Arabidopsis* homolog of SWI3, a core subunit of yeast Swi/Snf chromatin remodeling complex, interacts with FCA, a regulator of flowering time. *Nucleic Acids Res.* **30**, 3412–3421 (2002).
20. Vercruyssen, L. et al. ANGUSTIFOLIA3 binds to SWI/SNF chromatin remodeling complexes to regulate transcription during *Arabidopsis* leaf development. *Plant Cell* **26**, 210–229 (2014).
21. Wang, Z. et al. LFR, which encodes a novel nuclear-localized Armadillo-repeat protein, affects multiple developmental processes in the aerial organs in *Arabidopsis*. *Plant Mol. Biol.* **69**, 121 (2009).
22. Yu, Y. et al. BRAHMA-interacting proteins BRIP1 and BRIP2 are core subunits of *Arabidopsis* SWI/SNF complexes. *Nat. Plants* **6**, 996–1007 (2020).
23. Yu, Y. et al. Bromodomain-containing proteins BRD1, BRD2, and BRD13 are core subunits of SWI/SNF complexes and vital for their genomic targeting in *Arabidopsis*. *Mol. Plant* **14**, 888–904 (2021).
24. Jaronczyk, K. et al. Bromodomain-containing subunits BRD1, BRD2, and BRD13 are required for proper functioning of SWI/SNF complexes in *Arabidopsis*. *Plant Commun.* **2**, 100174 (2021).
25. Shang, J. Y. et al. COMPASS functions as a module of the INO80 chromatin remodeling complex to mediate histone H3K4 methylation in *Arabidopsis*. *Plant Cell* **33**, 3250–3271 (2021).
26. Luo, Y.-X. et al. A plant-specific SWR1 chromatin-remodeling complex couples histone H2A.Z deposition with nucleosome sliding. *EMBO J.* **39**, e102008 (2020).
27. Tan, L. M. et al. The PEAT protein complexes are required for histone deacetylation and heterochromatin silencing. *EMBO J.* **37**, e98770 (2018).
28. Bieluszewski, T. et al. AtEAF1 is a potential platform protein for *Arabidopsis* NuA4 acetyltransferase complex. *BMC Plant Biol.* **15**, 75 (2015).
29. Qi, D. et al. OSLFR is essential for early endosperm and embryo development by interacting with SWI/SNF complex members in *Oryza sativa*. *Plant J.* **104**, 901–916 (2020).
30. Hurtado, L., Farrona, S. & Reyes, J. C. The putative SWI/SNF complex subunit BRAHMA activates flower homeotic genes in *Arabidopsis thaliana*. *Plant Mol. Biol.* **62**, 291–304 (2006).
31. Sacharowski, S. P. et al. SWP73 subunits of *Arabidopsis* SWI/SNF chromatin remodeling complexes play distinct roles in leaf and flower development. *Plant Cell* **27**, 1889–1906 (2015).
32. Sarnowski, T. J. et al. SWI3 subunits of putative SWI/SNF chromatin-remodeling complexes play distinct roles during *Arabidopsis* development. *Plant Cell* **17**, 2454–2472 (2005).
33. Lin, X. et al. LFR physically and genetically interacts with SWI/SNF component SWI3B to regulate leaf blade development in *Arabidopsis*. *Front. Plant Sci.* **12**, 717649 (2021).
34. Wagner, F. R. et al. Structure of SWI/SNF chromatin remodeler RSC bound to a nucleosome. *Nature* **579**, 448–451 (2020).
35. Ye, Y. et al. Structure of the RSC complex bound to the nucleosome. *Science* **366**, 838–843 (2019).
36. He, S. et al. Structure of nucleosome-bound human BAF complex. *Science* **367**, 875–881 (2020).
37. Su, Y. H. et al. The N-terminal ATPase AT-hook-containing region of the *Arabidopsis* chromatin-remodeling protein SPLAYED is sufficient for biological activity. *Plant J.* **46**, 685–699 (2006).
38. Han, Y., Reyes, A. A., Malik, S. & He, Y. Cryo-EM structure of SWI/SNF complex bound to a nucleosome. *Nature* **579**, 452–455 (2020).
39. Mashtalir, N. et al. A structural model of the endogenous human BAF complex informs disease mechanisms. *Cell* **183**, 802–817 (2020).
40. Han, W. et al. The SWI/SNF subunit SWI3B regulates IAMT1 expression via chromatin remodeling in *Arabidopsis* leaf development. *Plant Sci.* **271**, 127–132 (2018).
41. Lin, X. et al. LFR is functionally associated with AS2 to mediate leaf development in *Arabidopsis*. *Plant J.* **95**, 598–612 (2018).
42. Li, C. et al. The *Arabidopsis* SWI2/SNF2 chromatin remodeler BRAHMA regulates polycomb function during vegetative development and directly activates the flowering repressor gene SVP. *PLoS Genet.* **11**, e1004944 (2015).
43. Farrona, S. et al. Brahma is required for proper expression of the floral repressor FLC in *Arabidopsis*. *PLoS ONE* **6**, e17997 (2011).
44. Archacki, R. et al. *Arabidopsis* SWI/SNF chromatin remodeling complex binds both promoters and terminators to regulate gene expression. *Nucleic Acids Res.* **45**, 3116–3129 (2017).
45. Guo, J. et al. The CBP/p300 histone acetyltransferases function as plant-specific MEDiator subunits in *Arabidopsis*. *J. Integr. Plant Biol.* **63**, 755–771 (2020).
46. Zhao, N. et al. The RNA recognition motif-containing protein UBA2c prevents early flowering by promoting transcription of the flowering repressor FLM in *Arabidopsis*. *N. Phytol.* **233**, 751–765 (2022).
47. Eberharter, A. & Becker, P. B. Histone acetylation: a switch between repressive and permissive chromatin. *EMBO Rep.* **3**, 224–229 (2002).
48. Zhang, X., Bernatavichute, Y. V., Cokus, S., Pellegrini, M. & Jacobsen, S. E. Genome-wide analysis of mono-, di- and

- trimethylation of histone H3 lysine 4 in *Arabidopsis thaliana*. *Genome Biol.* **10**, R62 (2009).
49. Zhang, X. et al. Whole-genome analysis of histone H3 lysine 27 trimethylation in *Arabidopsis*. *PLoS Biol.* **5**, e129 (2007).
  50. Zhao, S., Zhang, B., Yang, M., Zhu, J. & Li, H. Systematic profiling of histone readers in *Arabidopsis thaliana*. *Cell Rep.* **22**, 1090–1102 (2018).
  51. Tan, L.-M. et al. Dual recognition of H3K4me3 and DNA by the ISWI component ARID5 regulates the floral transition in *Arabidopsis*. *Plant Cell.* **32**, 2178–2195 (2020).
  52. Yang, Z. et al. EBS is a bivalent histone reader that regulates floral phase transition in *Arabidopsis*. *Nat. Genet.* **50**, 1247–1253 (2018).
  53. Qian, S. et al. Dual recognition of H3K4me3 and H3K27me3 by a plant histone reader SHL. *Nat. Commun.* **9**, 2425 (2018).
  54. López-González, L. et al. Chromatin-dependent repression of the *Arabidopsis* floral integrator genes involves plant specific PHD-containing proteins. *Plant Cell* **26**, 3922–3938 (2014).
  55. Heinz, S. et al. Simple combinations of lineage-determining transcription factors prime cis-regulatory elements required for macrophage and B cell identities. *Mol. Cell* **38**, 576–589 (2010).
  56. Torres, E. S. & Deal, R. B. The histone variant H2A.Z and chromatin remodeler BRAHMA act coordinately and antagonistically to regulate transcription and nucleosome dynamics in *Arabidopsis*. *Plant J.* **99**, 144–162 (2019).
  57. Hernández-García, J. et al. Comprehensive identification of SWI/SNF complex subunits underpins deep eukaryotic ancestry and reveals new plant components. *Commun. Biol.* **5**, 549 (2022).
  58. Chatterjee, N. et al. Histone acetylation near the nucleosome dyad axis enhances nucleosome disassembly by RSC and SWI/SNF. *Mol. Cell. Biol.* **35**, 4083–4092 (2015).
  59. Mashtalir, N. et al. Chromatin landscape signals differentially dictate the activities of mSWI/SNF family complexes. *Science* **373**, 306–315 (2021).
  60. Nakayama, R. T. et al. SMARCB1 is required for widespread BAF complex-mediated activation of enhancers and bivalent promoters. *Nat. Genet.* **49**, 1613–1623 (2017).
  61. Mittal, P. & Roberts, C. W. M. The SWI/SNF complex in cancer—biology, biomarkers and therapy. *Nat. Rev. Clin. Oncol.* **17**, 435–448 (2020).
  62. Zhu, B., Zhang, W., Zhang, T., Liu, B. & Jiang, J. Genome-wide prediction and validation of intergenic enhancers in *Arabidopsis* using open chromatin signatures. *Plant Cell* **27**, 2415–2426 (2015).
  63. Zeng, L. et al. Mechanism and regulation of acetylated histone binding by the tandem PHD finger of DPF3b. *Nature* **466**, 258–262 (2010).
  64. Ren, X. et al. Histone benzoylation serves as an epigenetic mark for DPF and YEATS family proteins. *Nucleic Acids Res.* **49**, 114–126 (2021).
  65. Local, A. et al. Identification of H3K4me1-associated proteins at mammalian enhancers. *Nat. Genet.* **50**, 73–82 (2018).
  66. Yan, W. et al. Dynamic control of enhancer activity drives stage-specific gene expression during flower morphogenesis. *Nat. Commun.* **10**, 1705 (2019).
  67. Zaret, K. S. & Mango, S. E. Pioneer transcription factors, chromatin dynamics, and cell fate control. *Curr. Opin. Genet. Dev.* **37**, 76–81 (2016).
  68. Pajoro, A. et al. Dynamics of chromatin accessibility and gene regulation by MADS-domain transcription factors in flower development. *Genome Biol.* **15**, R41 (2014).
  69. Jin, R. et al. LEAFY is a pioneer transcription factor and licenses cell reprogramming to floral fate. *Nat. Commun.* **12**, 626 (2021).
  70. Efroni, I. et al. Regulation of leaf maturation by chromatin-mediated modulation of cytokinin responses. *Dev. Cell* **24**, 438–445 (2013).
  71. Wu, M.-F. et al. SWI2/SNF2 chromatin remodeling ATPases overcome polycomb repression and control floral organ identity with the LEAFY and SEPALLATA3 transcription factors. *Proc. Natl Acad. Sci. USA* **109**, 3576–3581 (2012).
  72. Zhao, M. et al. Arabidopsis BREVIPEDICELLUS interacts with the SWI2/SNF2 chromatin remodeling ATPase BRAHMA to regulate KNAT2 and KNAT6 expression in control of inflorescence architecture. *PLoS Genet.* **11**, e1005125 (2015).
  73. Zhang, D., Li, Y., Zhang, X., Zha, P. & Lin, R. The SWI2/SNF2 chromatin-remodeling ATPase BRAHMA regulates chlorophyll biosynthesis in *Arabidopsis*. *Mol. Plant* **10**, 155–167 (2017).
  74. Zhang, W., Zhang, T., Wu, Y. & Jiang, J. Genome-wide identification of regulatory DNA elements and protein-binding footprints using signatures of open chromatin in *Arabidopsis*. *Plant Cell* **24**, 2719–2731 (2012).
  75. Maher, K. A. et al. Profiling of accessible chromatin regions across multiple plant species and cell types reveals common gene regulatory principles and new control modules. *Plant Cell* **30**, 15–36 (2018).
  76. Wang, F.-X. et al. Chromatin accessibility dynamics and a hierarchical transcriptional regulatory network structure for plant somatic embryogenesis. *Dev. Cell* **54**, 742–757, e8 (2020).
  77. Farmer, A., Thibivilliers, S., Ryu, K. H., Schiebelbein, J. & Libault, M. Single-nucleus RNA and ATAC sequencing reveals the impact of chromatin accessibility on gene expression in *Arabidopsis* roots at the single-cell level. *Mol. Plant* **14**, 372–383 (2021).
  78. Wang, Z.-P. et al. Egg cell-specific promoter-controlled CRISPR/Cas9 efficiently generates homozygous mutants for multiple target genes in *Arabidopsis* in a single generation. *Genome Biol.* **16**, 1–12 (2015).
  79. Nishimura, A., Aichi, I. & Matsuoka, M. A protocol for *Agrobacterium*-mediated transformation in rice. *Nat. Protoc.* **1**, 2796 (2006).
  80. Kim, D., Langmead, B. & Salzberg, S. L. HISAT: a fast spliced aligner with low memory requirements. *Nat. Methods* **12**, 357–360 (2015).
  81. Liao, Y., Smyth, G. K. & Shi, W. featureCounts: an efficient general purpose program for assigning sequence reads to genomic features. *Bioinformatics* **30**, 923–930 (2014).
  82. Robinson, M. D., McCarthy, D. J. & Smyth, G. K. edgeR: a Bioconductor package for differential expression analysis of digital gene expression data. *Bioinformatics* **26**, 139–140 (2010).
  83. Koldé, R. Pheatmap: pretty heatmaps (R package version 1, 2012).
  84. Warnes, G. R. et al. Gplots: various R programming tools for plotting data (R package version 2, 2014).
  85. Gendrel, A.-V., Lippman, Z., Martienssen, R. & Colot, V. Profiling histone modification patterns in plants using genomic tiling microarrays. *Nat. Methods* **2**, 213–218 (2005).
  86. Zhang, Y. et al. Model-based analysis of ChIP-seq (MACS). *Genome Biol.* **9**, R137 (2008).
  87. Ramírez, F. et al. deepTools2: a next generation web server for deep-sequencing data analysis. *Nucleic Acids Res.* **44**, W160–W165 (2016).
  88. Rossinnes, C. S. et al. Differential oestrogen receptor binding is associated with clinical outcome in breast cancer. *Nature* **481**, 389–393 (2011).
  89. Yu, G., Wang, L. G., Han, Y. & He, Q. Y. clusterProfiler: an R package for comparing biological themes among gene clusters. *OMICS* **16**, 284–287 (2012).
  90. Liu, W. et al. IBS: an illustrator for the presentation and visualization of biological sequences. *Bioinformatics* **31**, 3359–3361 (2015).
  91. Kumar, S., Stecher, G. & Tamura, K. MEGA7: molecular evolutionary genetics analysis version 7.0 for bigger datasets. *Mol. Biol. Evol.* **33**, 1870–1874 (2016).

## Acknowledgements

This work was supported by the National Natural Science Foundation of China (32025003) and by the National Key Research and Development Program of China (2016YFA0500801) from the Chinese Ministry of Science and Technology. We thank the Research Platform of Protein Science at Institute of Biophysics, Chinese Academy of Sciences, for providing the technical assistance on the ITC assay.

## Author contributions

J.G. (Beijing Normal University), G.C., Y.-X.Z., Z.-C.Z., Z.-Z.L., J.G. (National Institute of Biological Sciences), L.L. and S.C. performed the experiments. J.G. (Beijing Normal University), Y.-Q.L., Y.-N.S., D.-Y.Y. and X.-W.C. performed the bioinformatics analyses. J.G. (Beijing Normal University) and X.-J.H. designed the experiments. J.G. (Beijing Normal University) and X.-J.H. wrote the manuscript.

## Competing interests

The authors declare no competing interests.

## Additional information

**Extended data** is available for this paper at <https://doi.org/10.1038/s41477-022-01282-z>.

## Supplementary information

The online version contains supplementary material available at <https://doi.org/10.1038/s41477-022-01282-z>.

**Correspondence and requests for materials** should be addressed to Xin-Jian He.

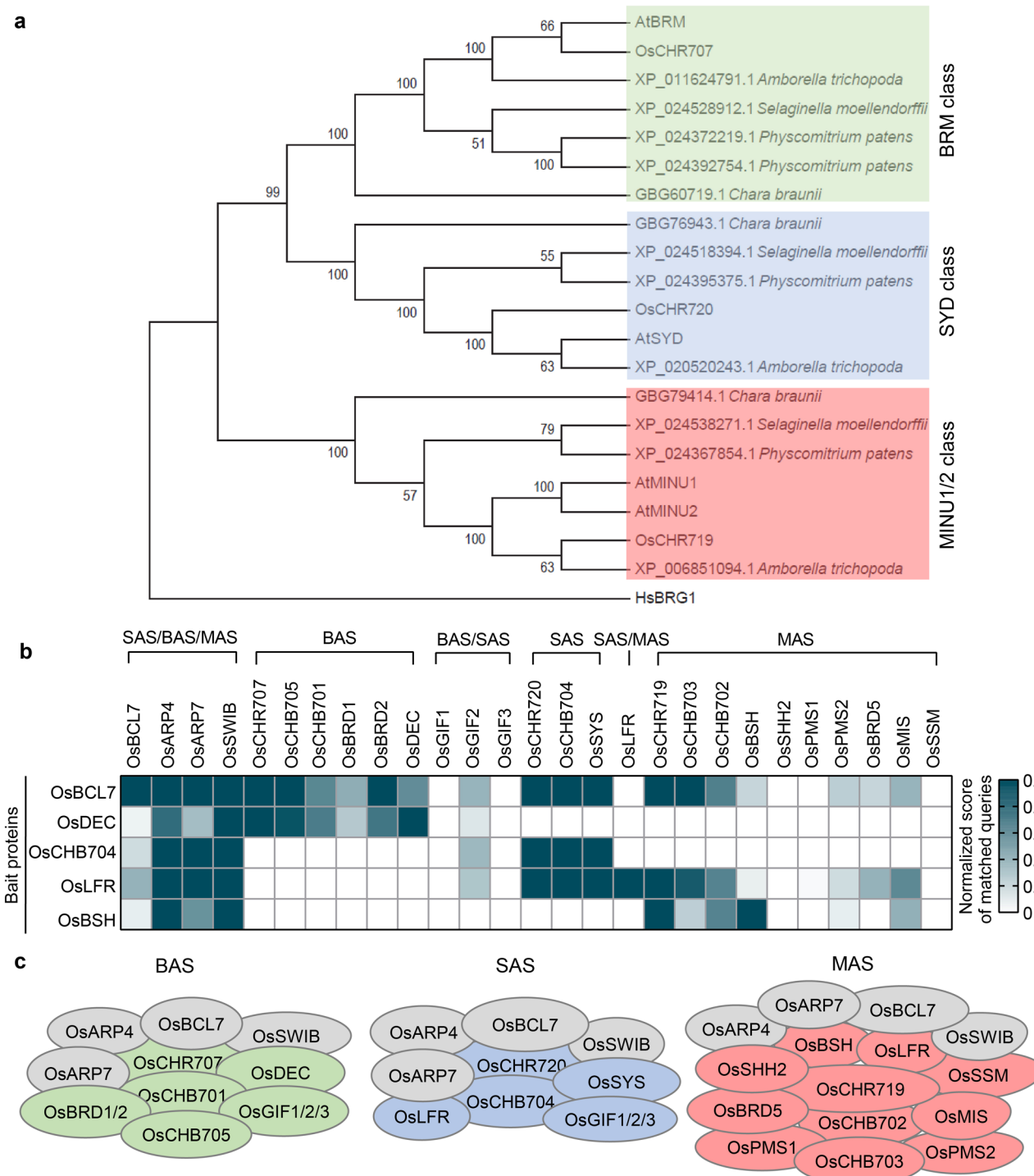
**Peer review information** *Nature Plants* thanks Sebastian Sacharowski and the other, anonymous, reviewer(s) for their contribution to the peer review of this work.

**Reprints and permissions information** is available at [www.nature.com/reprints](http://www.nature.com/reprints).

**Publisher's note** Springer Nature remains neutral with regard to jurisdictional claims in published maps and institutional affiliations.

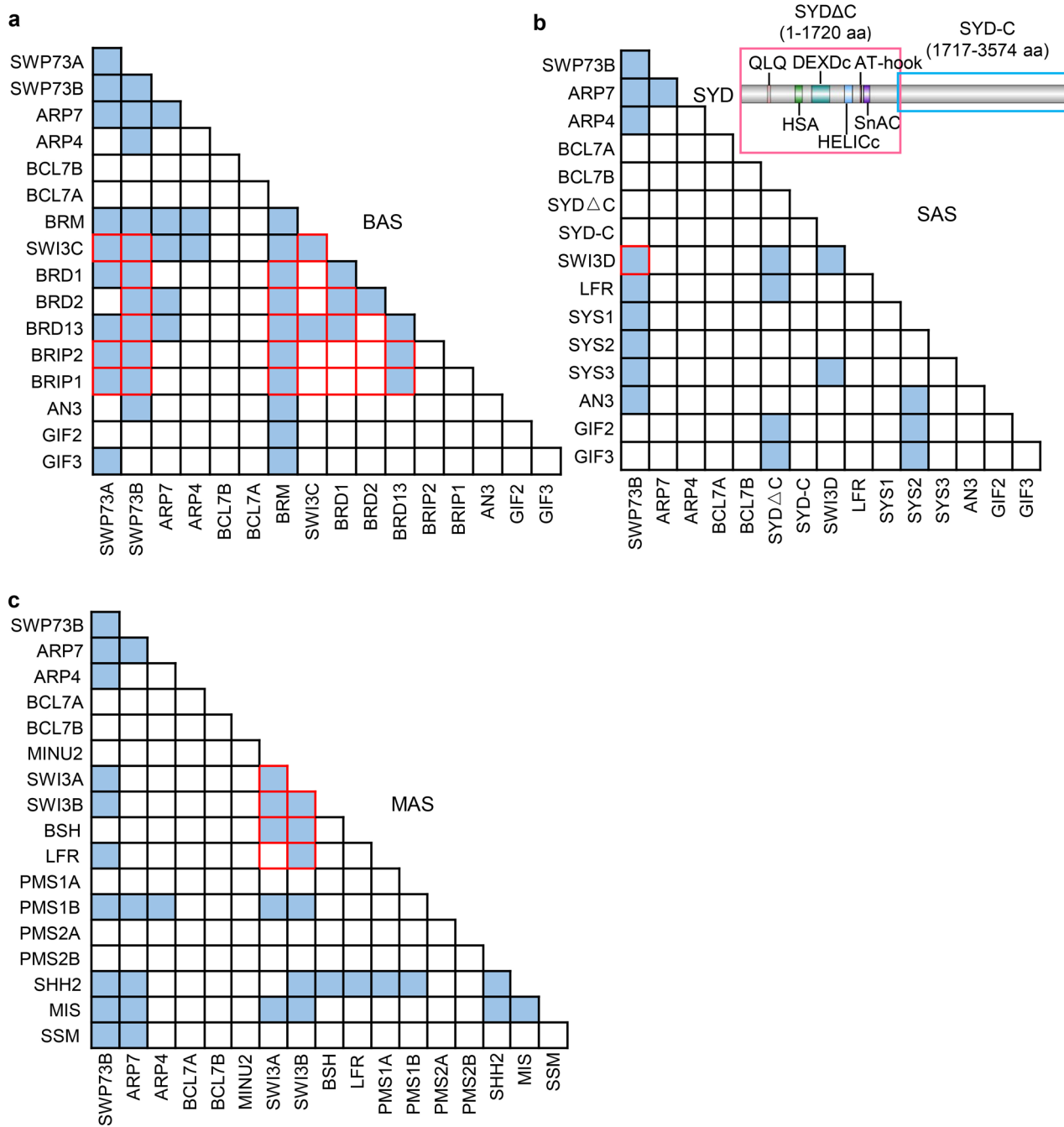
Springer Nature or its licensor (e.g. a society or other partner) holds exclusive rights to this article under a publishing agreement with the author(s) or other rightsholder(s); author self-archiving of the accepted manuscript version of this article is solely governed by the terms of such publishing agreement and applicable law.

© The Author(s), under exclusive licence to Springer Nature Limited 2022



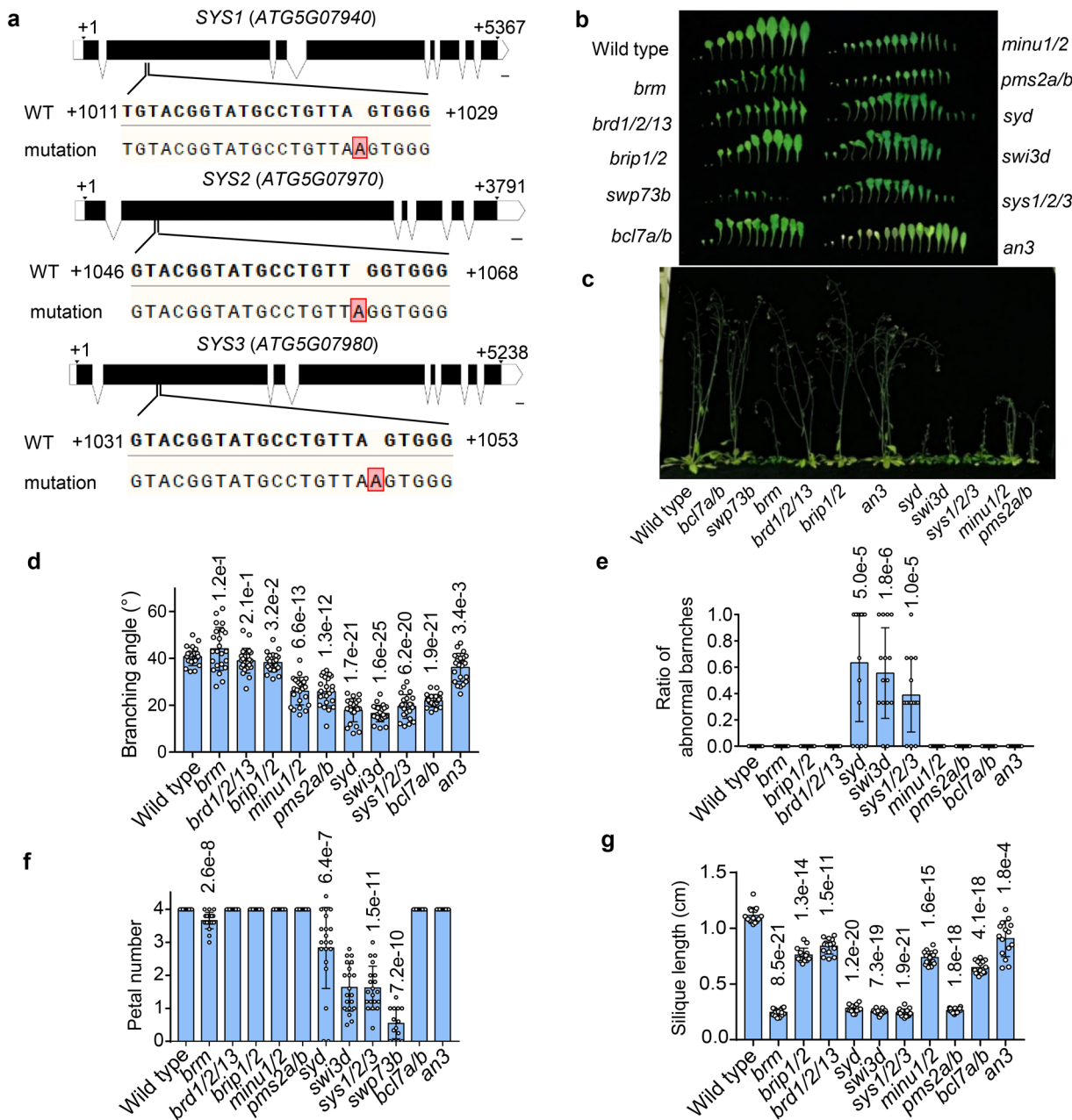
**Extended Data Fig. 1 | Phylogenetic analysis of SWI/SNF chromatin remodelers in different plant species and identification of SWI/SNF complexes in *Oryza sativa*.** **a**, A neighbor-joining tree was generated using the full-length protein sequences of BRM, SYD, MINU1, MINU2, and their orthologues in different plant species. The human SWI/SNF chromatin remodeler BRG1 was introduced as the outgroup. Bootstrap values: % invariant branches during resampling. **b**, Heatmap visualization of proteins co-purified with

GFP-tagged OsBCL7, OsDEC, OsCHB704, OsLFR and OsBSH as determined by AP-MS. The matched queries of a prey protein are normalized by the average matched queries of the total subunits purified by a bait protein. **c**, Schematic representations of BAS, SAS and MAS complexes in *Oryza sativa*. Shared subunits are shown in grey. Specific subunits of BAS, SAS and MAS complexes are shown in green, blue and red, respectively.



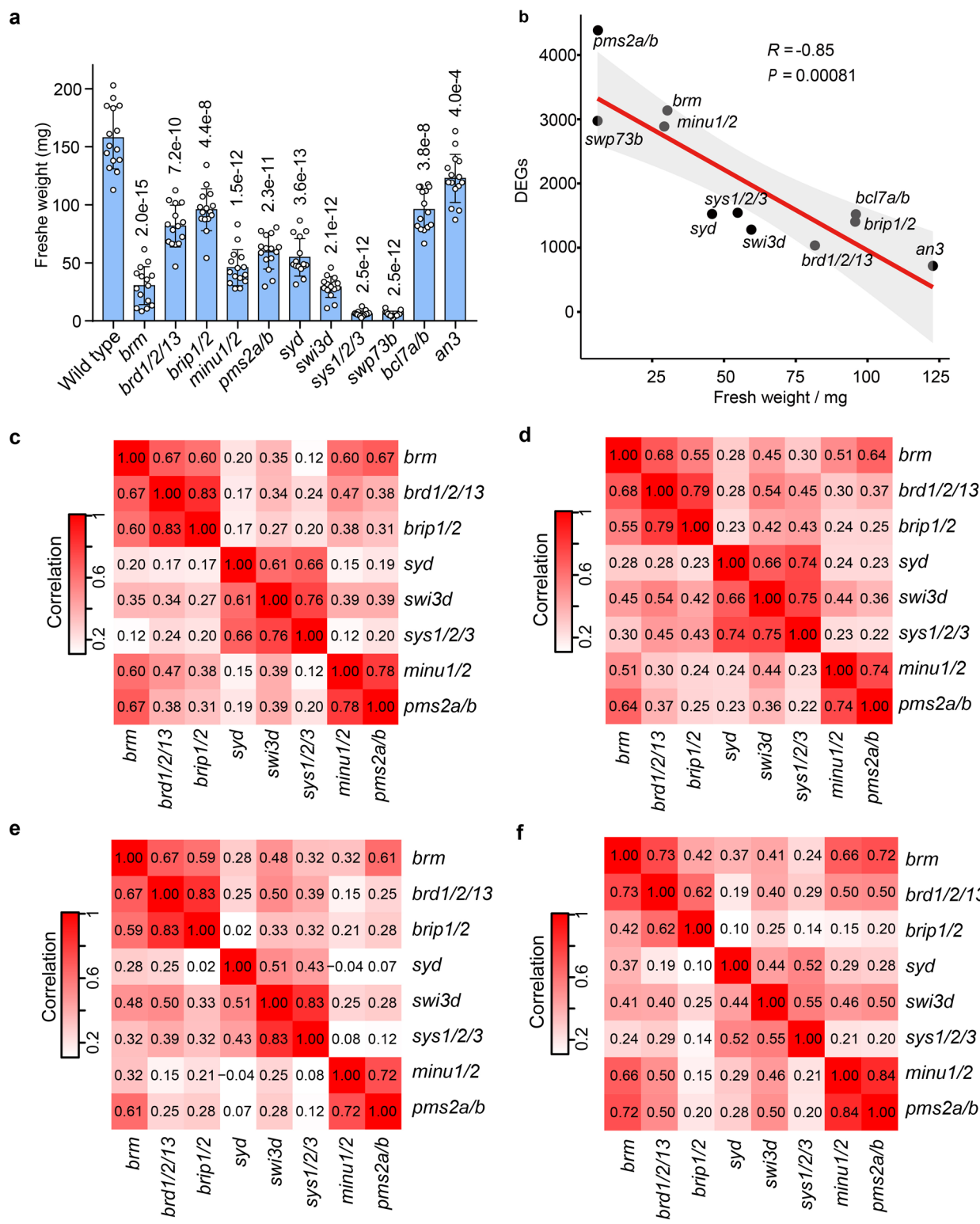
**Extended Data Fig. 2 | Interactions between subunits of BAS, SAS, and MAS complexes as determined by Y2H assays.** **a**, Interactions of BAS complex subunits. The truncated versions of BRM used in Y2H assays. **b**, Interactions of SAS complex subunits. The truncated SYD versions SYD $\Delta$ C and SYD-C used in

Y2H assays are shown on the top panel. **c**, Interaction of MAS complex subunits. The interactions detected by Y2H assays in this study are highlighted in blue, and the previously published interactions are labelled by red frames. Blank boxes indicate that no interaction was detected.



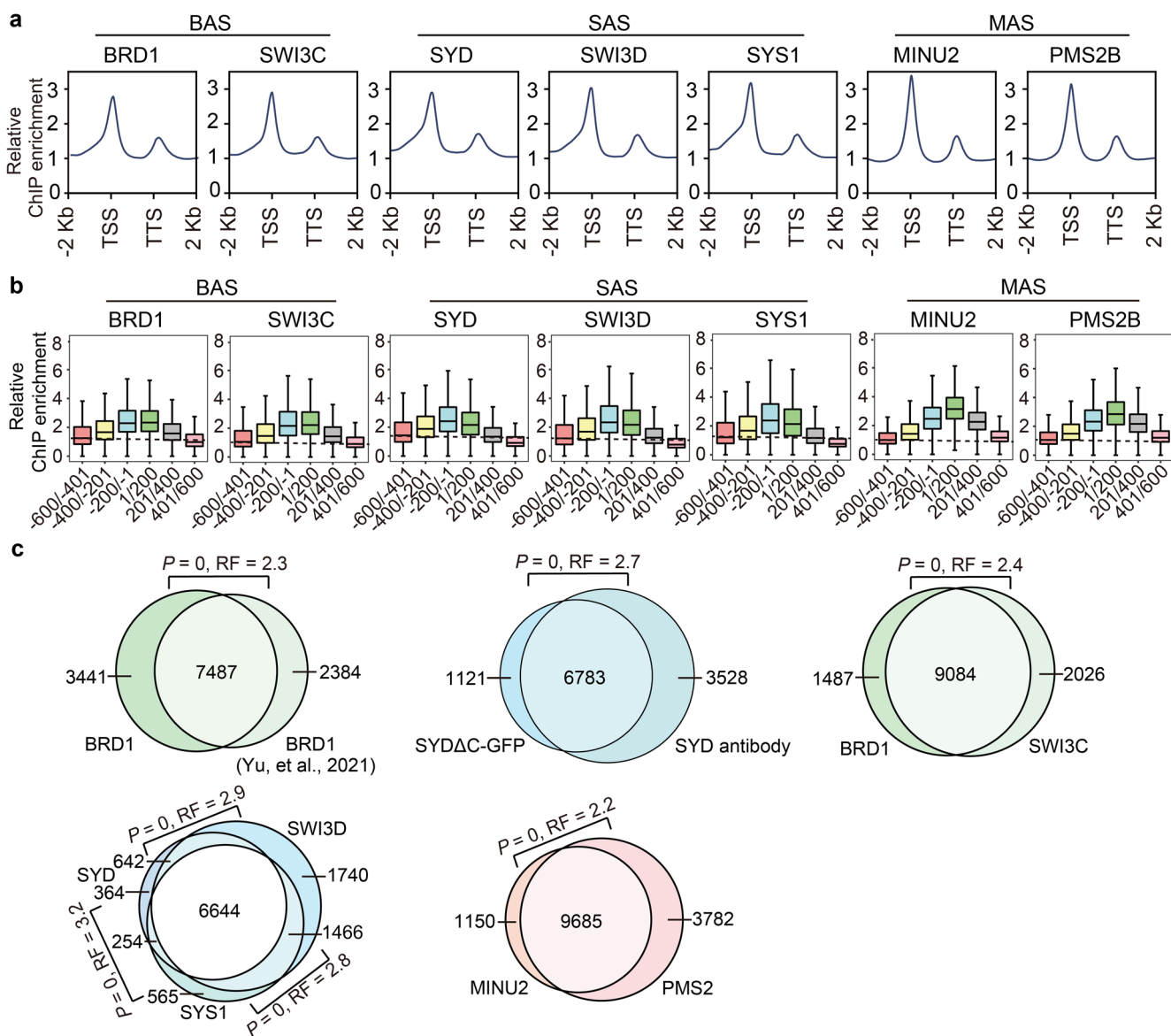
**Extended Data Fig. 3 | Developmental phenotypes of SWI/SNF mutants. a,** Schematic representations of mutations in *SYS1*, *SYS2* and *SYS3* mediated by CRISPR/Cas9. The translation start sites are marked by +1. The untranslated regions (UTR) and exon regions are indicated with blank and black boxes, respectively. Introns are indicated with fold lines. The mutations validated by Sanger sequencing are illustrated by red boxes. WT: wild type. Scale bar: 100 bp. **b**, Morphological phenotypes of cotyledons and rosette leaves taken from bolting plants of SWI/SNF mutants and wild type. **c**, Morphological phenotypes of 5-week-old plants of SWI/SNF mutants and wild type. **d**, Measurement of the first cauline branching angles in indicated genotypes. P values determined by two-tailed Student's t-test or Welch's t-test indicate the difference between the mutants and the wild-type control. n = 23. **e**, The ratio of abnormal cauline

branches of which the growth positions are not at the axils of caulin leaves. n = 15. P values determined by two-tailed Mann Whitney U test indicate the difference between the mutants and the wild-type control. **f**, Petal number in the indicated genotypes. The average petal number of five flowers was calculated for each plant. The petal numbers of 20 plants were determined for each genotype (except for *swp73b*, n = 14). P values determined by two-tailed Mann Whitney U test indicate the difference between the mutants and the wild-type control. **g**, The average length of all the siliques from the main stem was determined for each plant. n = 15. P values determined by two-tailed Student's t-test or Welch's t-test indicate the difference between the mutants and the wild-type control. Data are presented as mean values +/- SD in **d-g**.



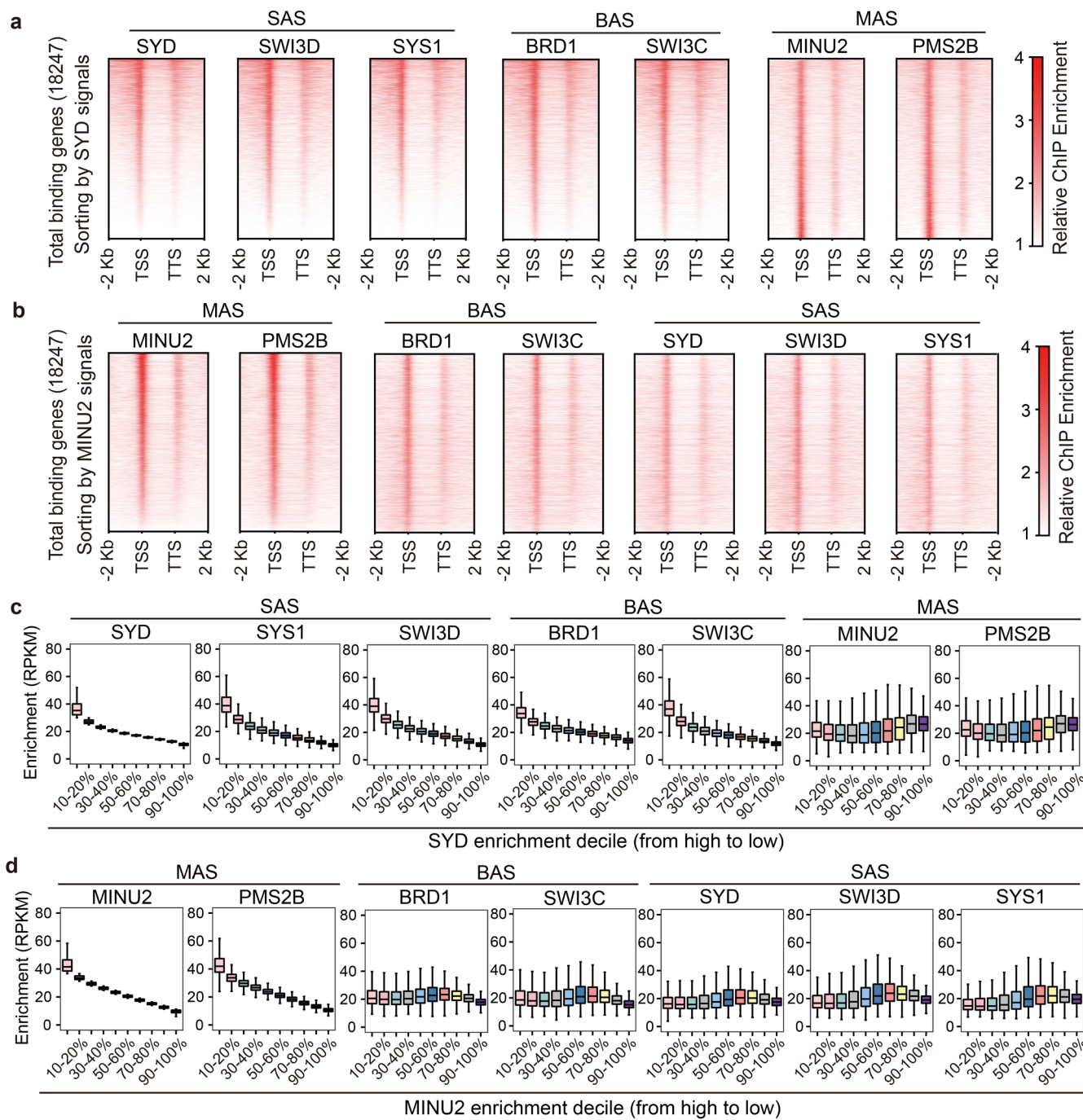
**Extended Data Fig. 4 | Comparison of the effects of SWI/SNF mutations on development and gene expression.** **a**, Fresh weight of 23-day-old plants of SWI/SNF mutants and wild type. The fresh weight of 15 plants were determined for each genotype. *P* values determined by two-tailed Student's *t*-test or Welch's *t*-test indicate the difference between the mutants and the wild-type control. Data are presented as mean values  $\pm$  SD. **b**, Scatter plot with a fitted regression line and a 95% confidence interval band showing the correlation between the plant fresh weight and the differentially expressed genes in SWI/SNF mutants.

*R* represents the Pearson correlation coefficient. *P* value were determined by two-tailed *t*-test. **c-f**, Determination of the correlation of development-related differentially expressed genes between different SWI/SNF mutants. Heatmaps show the Pearson Correlation Coefficient of *brm*, *brd1/2/13*, *brip1/2*, *syd*, *swi3d*, *sys1/2/3*, *minu1/2*, *pms2a/b* based on the expression changes of leaf development-related genes (**c**), flower development-related genes (**d**), flowering time-related genes (**e**), and embryo development-related genes (**f**).



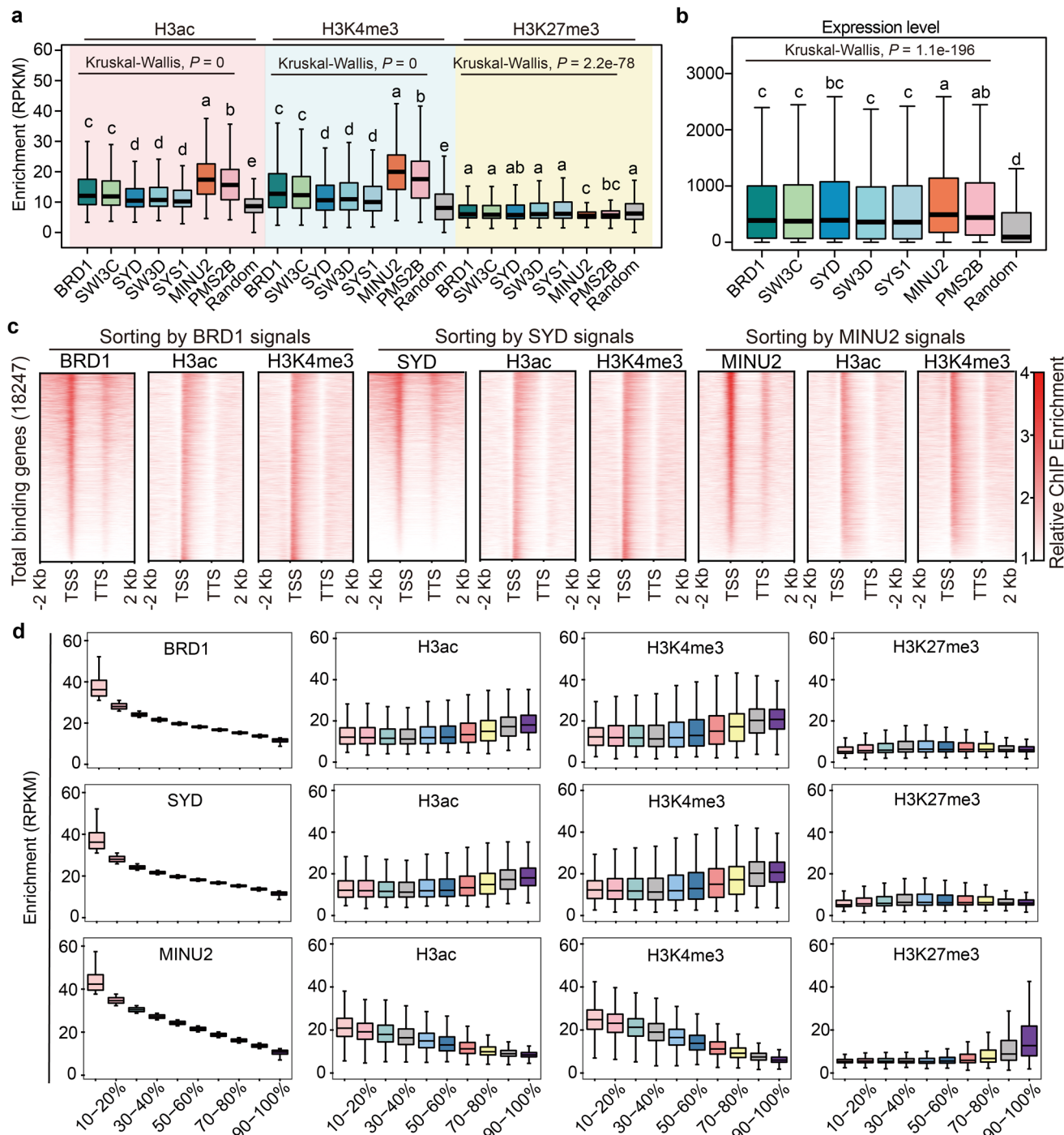
**Extended Data Fig. 5 | Comparison of BAS-, SAS- and MAS-occupied TSS-flanking regions and genes as determined by ChIP-seq.** **a**, Profile plots showing the enrichment of the SWI/SNF components at the genes bound by each component. **b**, Boxplots showing the enrichment of SWI/SNF components at the TSS-flanking region of their binding genes. The enrichment of SWI/SNF components was calculated at 200-bp bins of the TSS-flanking region. Sample size of each box plot: BRD1 ( $n = 10928$ ), SWI3C ( $n = 11110$ ), SYD ( $n = 7904$ ), SWI3D ( $n = 10492$ ), SYS1 ( $n = 8929$ ), MINU2 ( $n = 10835$ ), PMS2B ( $n = 13467$ ). In

box plots, center lines and box edges are medians and the interquartile range (IQR), respectively. Whiskers extend within 1.5 times the IQR. **c**, Venn diagrams showing the overlap of genes occupied by indicated SWI/SNF components. The overlapping significance is shown by  $P$  values as determined by hypergeometric test (one-tailed). RF (representation factor) represents the number of overlapping genes divided by the expected number of overlapping genes drawn from two independent groups.



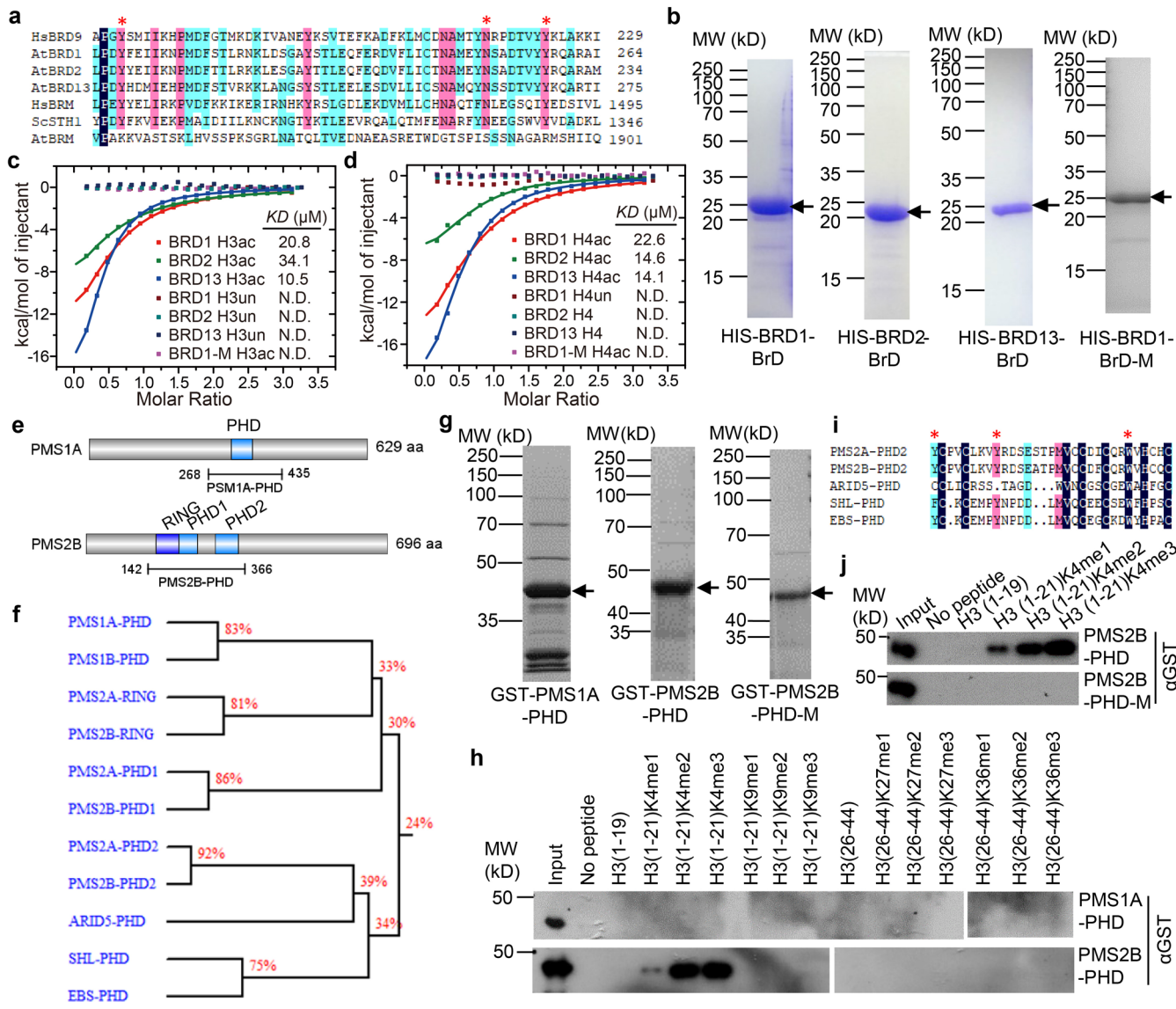
**Extended Data Fig. 6 | Determination of the correlation between the enrichments of BAS, SAS and MAS components at chromatin.** **a, b**, Heatmaps showing the enrichment of indicated SWI/SNF components at all the SWI/SNF components-occupied genes. The genes are subjected to sorting by the maximum enrichment value of each region of SYD (**a**) and MINU2 (**b**) at these

genes. **c, d**, Enrichment of indicated SWI/SNF components at SYD (**c**) and MINU2 (**d**) enrichment deciles of the total regions ( $n = 18552$ ) occupied by SWI/SNF components. In box plots of **c** and **d**, center lines and box edges are medians and the interquartile range (IQR), respectively. Whiskers extend within 1.5 times the IQR.



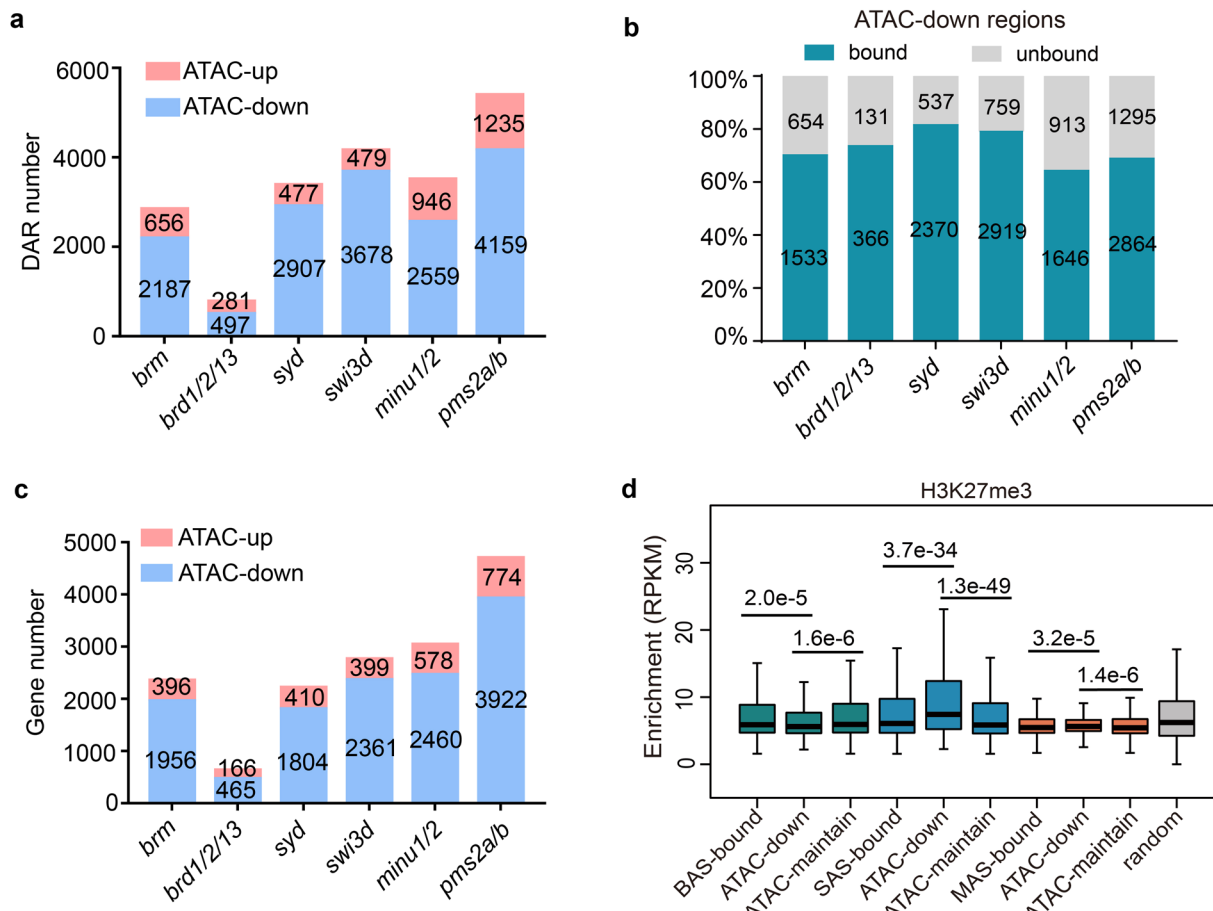
**Extended Data Fig. 7 | The histone modification and expression levels of genes occupied by BAS, SAS and MAS components.** **a**, The H3ac, H3K4me3, and H3K27me3 levels at regions occupied by indicated BAS, SAS, and MAS components in the wild-type plants. The sample size of each boxplot: BRD1 ( $n = 12973$ ), SWI3C ( $n = 13851$ ), SYD ( $n = 9687$ ), SWI3D ( $n = 13099$ ), SYS1 ( $n = 11875$ ), MINU2 ( $n = 11729$ ), PMS2B ( $n = 15207$ ), random ( $n = 10000$ ).  $P$  values for Kruskal-Wallis tests indicate the differences of the histone modification levels within a group (marked by black lines). Lowercase letters above the boxplots show the results of Dunnett's test, with statistically similar clusters grouped by the same letter. **b**, The expression levels of genes occupied by indicated BAS, SAS, and MAS components in the wild-type plants. The sample size of each boxplot: BRD1 ( $n = 12973$ ), SWI3C ( $n = 13851$ ), SYD ( $n = 9687$ ), SWI3D ( $n = 13099$ ), SYS1 ( $n = 11875$ ),

MINU2 ( $n = 11729$ ), PMS2B ( $n = 15207$ ), random ( $n = 10000$ ).  $P$  values for Kruskal-Wallis tests indicate the expression differences within a group (marked by black lines). Lowercase letters above the boxplots show the results of Dunnett's test, with statistically similar clusters grouped by the same letter. **c**, Heatmap showing the enrichment of H3ac and H3K4me3 at all the SWI/SNF components-occupied genes. The genes are subjected to sorting by the maximum enrichment value of BRD1 (left), SYD (middle), and MINU2 (right)-occupied regions. **d**, Enrichment of H3ac, H3K4me3, and H3K27me3 at BRD1, SYD and MINU2 enrichment deciles of total regions ( $n = 18552$ ) occupied by SWI/SNF components. In box plots of **a**, **b** and **d**, center lines and box edges are medians and the interquartile range (IQR), respectively. Whiskers extend within 1.5 times the IQR.



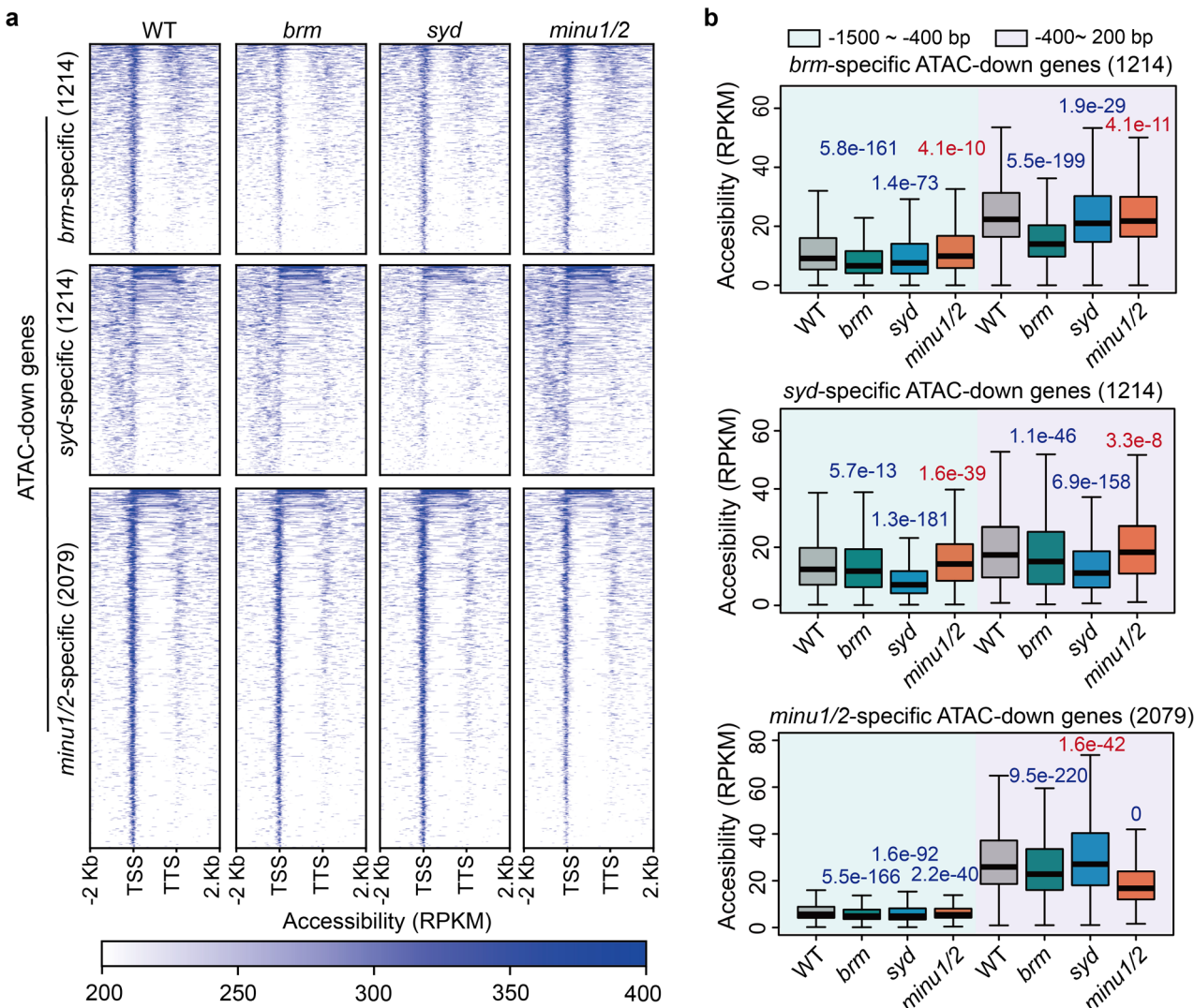
**Extended Data Fig. 8 | The bromodomains of BRD1, BRD2 and BRD13 bind to acetylated histones and the second PHD domain of PMS2B binds to methylated H3 at lysine 4.** **a**, Sequence alignment of the bromodomains of HsBRD9, AtBRD1, AtBRD2, AtBRD13, HsBRM, ScSTH1, and AtBRM. The BRD1 bromodomain conserved residues Y207, N251 and Y258 marked with asterisks were subjected to point mutation. **b**, Coomassie blue staining of the wild-type BRD1, BRD2, and BRD13 bromodomains and of the mutated BRD1 bromodomain (BRD1-M) tagged by HIS. The fusion proteins were purified from *E. coli*. The experiments were repeated for at least two times with similar results. **c,d**, ITC binding assays measuring the binding affinity of the bromodomains of BRD1, BRD2, BRD13 and BRD1-M for acetylated and unmodified H3 peptides (**c**) and acetylated and unmodified H4 peptides (**d**). **e**, Schematic representations indicate the domain architecture of PMS1A and PMS2B and the truncated versions of PMS1A and PMS2B purified from *E. coli*. **f**, A phylogenetic tree of the PHD domains in PMS1A, PMS1B, PMS2A, PMS2B, and in the known PHD-containing H3K4me3 readers ARID5, SHL and EBS. The RING fingers of PMS2A

and PMS2B that are closely related to the conserved PHD finger were included for analysis. **g**, Coomassie blue staining of the wild-type PMS1A and PMS2B PHD domains and of the mutated PMS2B PHD domain tagged by GST. The proteins were expressed and purified from *E. coli*. The experiments were repeated for at least two times with similar results. **h**, Determination of the binding of wild-type PMS1A and PMS2B PHD domains to methylated and unmethylated histone peptides by *in vitro* binding assays. **i**, Sequence alignment of the second PHD fingers of PMS2A and PMS2B (PMS2A-PHD2 and PMS2B-PHD2) and the PHD fingers of ARID5, SHL and EBS. Three conserved aromatic residues (Y148, Y155, and W170) in the PMS2B-PHD2 marked with asterisks were mutated to alanine in the mutated version of PMS2B (PMS2B-PHD-M). The experiment was repeated for two times with similar results. **j**, The effect of the PMS2B-PHD2 mutation on the binding ability of PMS2B for methylated H3 at lysine 4 as determined by *in vitro* binding assays. The experiment was repeated for two times with similar results.



**Extended Data Fig. 9 | Different effects of BAS, SAS and MAS mutations on chromatin accessibility.** **a**, The number of differential accessible regions (DARs) in indicated SWI/SNF mutants. DARs with increased accessibility (ATAC-up) were represented in red and DARs with decreased accessibility (ATAC-down) were represented in blue. **b**, The percentage of BAS/SAS/MAS-bound and unbound regions among the regions with decreased accessibility (ATAC-down regions) in corresponding BAS/SAS/MAS mutants. **c**, The number of genes with increased accessibility and genes with decreased accessibility in indicated SWI/SNF mutants. Genes with increased accessibility (ATAC-up) were represented in red and genes with decreased accessibility (ATAC-down) were represented

in blue. **d**, Boxplots showing H3K27me3 levels at the regions bound by each complex and the regions bound by each complex with decreased (ATAC-down) or maintained (ATAC-maintain) accessibility. The sample size of each box plot: BAS-bound (n = 12392), ATAC-down (n = 1470), ATAC-maintain (n = 10922), SAS-bound (n = 11398), ATAC-down (n = 2195), ATAC-maintain (n = 9203), MAS-bound (n = 11129), ATAC-down (n = 1637), ATAC-maintain (n = 9492), random (n = 10000). In box plots, center lines and box edges are medians and the interquartile range (IQR), respectively. Whiskers extend within 1.5 times the IQR. P values determined by two-tailed Mann Whitney *U* test indicate the difference between indicated samples.



**Extended Data Fig. 10 | Different effects of BAS, SAS and MAS mutations on chromatin accessibility.** **a**, Heatmap depicting the effects of BAS, SAS, and MAS enzyme mutations on chromatin accessibility at genes whose chromatin accessibility is specifically reduced in *brm*, *syd*, and *minu1/2*. WT: wild type. **b**, Boxplots showing the chromatin accessibility levels in the *brm*, *syd* and *minu1/2* mutants and the wild type at the 400–1500 bp upstream region of TSS and at the –400–200-bp TSS-flanking region. Those genes with reduced

chromatin accessibility specifically in *brm*, *syd*, and *minu1/2* mutants were independently analyzed. In box plots, center lines and box edges are medians and the interquartile range (IQR), respectively. Whiskers extend within 1.5 times the IQR. *P* values determined by two-tailed Wilcoxon signed rank test indicate the difference between the mutants and the wild-type control. WT: wild type. *P* values of reduced and increased signals in indicated mutants are shown in blue and red, respectively.

Corresponding author(s): Xin-Jian He

Last updated by author(s): Oct 11, 2022

## Reporting Summary

Nature Portfolio wishes to improve the reproducibility of the work that we publish. This form provides structure for consistency and transparency in reporting. For further information on Nature Portfolio policies, see our [Editorial Policies](#) and the [Editorial Policy Checklist](#).

### Statistics

For all statistical analyses, confirm that the following items are present in the figure legend, table legend, main text, or Methods section.

n/a Confirmed

- The exact sample size ( $n$ ) for each experimental group/condition, given as a discrete number and unit of measurement
- A statement on whether measurements were taken from distinct samples or whether the same sample was measured repeatedly
- The statistical test(s) used AND whether they are one- or two-sided  
*Only common tests should be described solely by name; describe more complex techniques in the Methods section.*
- A description of all covariates tested
- A description of any assumptions or corrections, such as tests of normality and adjustment for multiple comparisons
- A full description of the statistical parameters including central tendency (e.g. means) or other basic estimates (e.g. regression coefficient) AND variation (e.g. standard deviation) or associated estimates of uncertainty (e.g. confidence intervals)
- For null hypothesis testing, the test statistic (e.g.  $F$ ,  $t$ ,  $r$ ) with confidence intervals, effect sizes, degrees of freedom and  $P$  value noted  
*Give P values as exact values whenever suitable.*
- For Bayesian analysis, information on the choice of priors and Markov chain Monte Carlo settings
- For hierarchical and complex designs, identification of the appropriate level for tests and full reporting of outcomes
- Estimates of effect sizes (e.g. Cohen's  $d$ , Pearson's  $r$ ), indicating how they were calculated

*Our web collection on [statistics for biologists](#) contains articles on many of the points above.*

### Software and code

Policy information about [availability of computer code](#)

#### Data collection

For mass spectrometry analysis, the peptides were sprayed into a Q Exactive Mass Spectrometer equipped with a nano-ESI ion source (Thermo Fisher Scientific, USA). Peptide sequence data identified by mass spectrometry were searched in the International Protein Index database of Arabidopsis and in the NCBI database of Oryza sativa on the Mascot server (Matrix Science, London, UK). Illumina Novaseq 6000 platform was used to determine ChIP-seq and ATAC-seq data, by a paired-end scheme (PE150). DNBSEQ platform was used to determine RNA-seq data, by a single-end scheme (SE50).

#### Data analysis

Mass spectrometry data were analyzed and generated using Microsoft Excel (office 365) and GraphPad prism (v7). **Barplots and statistics were done using GraphPad prism (v7).**  
RNA-seq data were analyzed using HISAT2 (v2.1.0), featureCounts (v2.0.0), edgeR (v3.28.1) and DeepTools (v3.4.3).  
ChIP-seq data were analyzed using Bowtie2 (v2.3.5.1), MACS2 (v2.2.7.1) and DeepTools (v3.4.3).  
ATAC-seq data were analyzed using Trim Galore (version 0.6.6), Bowtie2 (v2.3.5.1), MACS2 (v2.2.7.1), DeepTools (v3.4.3) and DiffBind (v2.16.0).  
The multi-dimensional scaling (MDS) plot was generated by the **plotMDS** function of edgeR (v3.28.1).  
The heatmap of DEGs was drawn using the R package **Pheatmap** (v1.0.12).  
The heatmap based on Pearson correlation coefficients was drawn using the **heatmap.2** function of the R package gplots (v 3.0.3).  
The profile plot and related heatmap were drawn using the **plotProfile** and **plotHeatmap** function of DeepTools (v3.5.1).  
The principle components analysis (PCA) plot was drawn using DiffBind (v2.16.0).  
Boxplots were drawn with the boxplot function in R (v4.1.0).  
GO analysis was done using ClusterProfiler (v3.16.1).  
Motif analysis was done using the findMotifsGenome.pl and scanMotifGenomeWide.pl program with default parameters in Homer (version 4.11.1).  
ITC data were analyzed using the Origin (v7.0).

Multiple sequence alignment and the homology tree generation were done by DNAMAN (v8). Phylogenetic tree was generated by MEGA (v7).

For manuscripts utilizing custom algorithms or software that are central to the research but not yet described in published literature, software must be made available to editors and reviewers. We strongly encourage code deposition in a community repository (e.g. GitHub). See the Nature Portfolio [guidelines for submitting code & software](#) for further information.

## Data

Policy information about [availability of data](#)

All manuscripts must include a [data availability statement](#). This statement should provide the following information, where applicable:

- Accession codes, unique identifiers, or web links for publicly available datasets
- A description of any restrictions on data availability
- For clinical datasets or third party data, please ensure that the statement adheres to our [policy](#)

A reporting summary for this paper is available as a Supplementary Information file. Source data are provided with this paper.

The GEO accession number is for RNA-seq, ChIP-seq, and ATAC-seq data.

These data contain:

1. ChIP-seq data: BRD1-input, BRD1\_IP\_rep1, BRD1\_IP\_rep2, SWI3C\_input, SWI3C\_IP\_rep1, SWI3C\_IP\_rep2, SYD\_input, SYD\_IP\_rep1, SYD\_IP\_rep2, SWI3D\_input, SWI3D\_IP\_rep1, SWI3D\_IP\_rep2, SYS1\_input, SYS1\_IP\_rep1, SYS1\_IP\_rep2, MINU2\_input, MINU2\_IP\_rep1, MINU2\_IP\_rep2, PMS2B\_input, PMS2B\_IP\_rep1, PMS2B\_IP\_rep2.
2. RNA-seq data: WT\_rep1, WT\_rep2, WT\_rep3, brm\_rep1, brm\_rep2, brm\_rep3, brd1/2/13\_rep1, brd1/2/13\_rep2, brd1/2/13\_rep3, brip1/2\_rep1, brip1/2\_rep2, brip1/2/rep3, syd\_rep1, syd\_rep2, syd\_rep3, swi3d\_rep1, swi3d\_rep2, swi3d\_rep3, minu1/2\_rep1, minu1/2\_rep2, minu1/2\_rep3, pms2a/b\_rep1, pms2a/b\_rep2, pms2a/b\_rep3, swp73b\_rep1, swp73b\_rep2, swp73b\_rep3, bcl7a/b\_rep1, bcl7a/b\_rep2, bcl7a/b\_rep3, an3\_rep1, an3\_rep2, an3\_rep3.
3. ATAC-seq data: WT\_rep1, WT\_rep2, brm\_rep1, brm\_rep2, brd1/2/13\_rep1, brd1/2/13\_rep2, syd\_rep1, syd\_rep2, swi3d\_rep1, swi3d\_rep2, minu1/2\_rep1, minu1/2\_rep2, pms2a/b\_rep1, pms2a/b\_rep2.

The link of the data is:

<https://www.ncbi.nlm.nih.gov/geo/query/acc.cgi?acc=GSE193397>

There are no restrictions on data availability in our manuscript.

The accession numbers of genes reported in this study are as follows:

AT3G01890 (SWP73A), AT5G14170 (SWP73B), AT4G22320 (BCL7A), AT5G55210 (BCL7B), AT1G18450 (ARP4), AT3G60830 (ARP7), AT2G46020 (BRM), AT1G21700 (SWI3C), AT1G20670 (BRD1), AT1G76380 (BRD2), AT5G55040 (BRD13), AT3G03460 (BRIP1), AT5G17510(BRIP2), AT5G28640 (AN3), AT1G01160 (GIF2), AT4G00850 (GIF3), AT2G28290 (SYD), AT4G34430 (SWI3D), AT5G07940 (SYS1), AT5G07970 (SYS2), AT5G07980 (SYS3), AT3G22990 (LFR), AT3G06010 (MINU1), AT5G19310 (MINU2), AT2G47620 (SWI3A), AT2G33610 (SWI3B), AT3G17590 (BSH), AT3G18380 (SHH2), AT1G50620 (PMS1A), AT3G20280 (PMS1B), AT3G08020 (PMS2A), AT3G52100 (PMS2B), AT1G58025 (BRD5), AT1G32730 (MIS), AT1G06500 (SSM), Os09g0284300 (OsBCL7), Os08g0137200 (OsARP4), Os03g0783000 (OsARP7), Os04g0382100 (OsSWIB), Os02g0114033 (OsCHR707), Os11g0183700 (OsSWI3C), Os12g0176700 (OsCHB701), Os03g0130800 (OsBRD1), Os09g0550000 (OsBRD2), Os12g0465700 (OsDEC), Os03g0733600 (OsGIF1), Os11g0615200 (OsGIF2), Os12g0496900 (OsGIF3), Os06g0255200 (OsCHR720), Os04g0110300 (OsCHB704), Os03g0213300 (OsSYS), Os07g0609766 (OsLFR), Os05g0144300 (OsCHR719), Os04g0480300 (OsCHB703), Os02g0194000 (OsCHB702), Os02g0723700 (OsBSH), Os06g0485100 (OsSHH2), Os06g0309000 (OsPMS1), Os12g0527800 (OsPMS2), Os08g0109500 (OsBRD5), Os08g0129500 (OsMIS), and Os01g0246500 (OsSSM).

## Field-specific reporting

Please select the one below that is the best fit for your research. If you are not sure, read the appropriate sections before making your selection.

Life sciences       Behavioural & social sciences       Ecological, evolutionary & environmental sciences

For a reference copy of the document with all sections, see [nature.com/documents/nr-reporting-summary-flat.pdf](https://nature.com/documents/nr-reporting-summary-flat.pdf)

## Life sciences study design

All studies must disclose on these points even when the disclosure is negative.

Sample size	Sample sizes were determined based on previous studies and experiments in the field. Sample size in all the experiments was sufficient for statistical significance and reproducibility. For the assessment of plant phenotypes, at least 14 plants were used for measurement. The exact sample size of each measurement was noted in the figure legend. For AP-MS, at least 200 Arabidopsis seedlings and 40 rice seedlings were used for each replicate. For RNA-seq, at least 5 seedlings were used for each replicate. For ChIP-seq, at least 300 seedlings were used for each replicate. For ATAC-seq, at least 10 seedlings were used for each replicate.
-------------	--

Data exclusions	No data were excluded.
-----------------	------------------------

Replication	For AP-MS, the results of most Arabidopsis samples and all the rice samples are replicated for more than one time from different attempts, and all the attempts of replication got similar results and support the composition of the complexes. For RNA-seq, three biological replicates were performed for each sample and the results of the replicates are identical. The RNA-seq experiment was attempted for two times, and the results are similar. For ChIP-seq, two biological replicates were performed, generating similar results.
-------------	--

For ATAC-seq, two biological replicates were performed, generating similar results.  
For protein purification, ITC assay, Western blot and RT-PCR, the experiments were repeated for two or three times with similar results.

**Randomization** Data were collected according to the genotype of plants. Plants of different genotypes were grown side by side in the identical conditions. The plants were randomly collected without bias.

**Blinding** Blinding was largely not relevant to our study. Data were collected according to the genotype of plants. There was no possible bias during the material collection, and blinding the samples during the experiments increases the risk of mislabeling and wrong results.

## Reporting for specific materials, systems and methods

We require information from authors about some types of materials, experimental systems and methods used in many studies. Here, indicate whether each material, system or method listed is relevant to your study. If you are not sure if a list item applies to your research, read the appropriate section before selecting a response.

### Materials & experimental systems

- |                                     |  |
|-------------------------------------|--|
| n/a                                 | Involved in the study                                  |
| <input type="checkbox"/>            | <input checked="" type="checkbox"/> Antibodies         |
| <input checked="" type="checkbox"/> | <input type="checkbox"/> Eukaryotic cell lines         |
| <input checked="" type="checkbox"/> | <input type="checkbox"/> Palaeontology and archaeology |
| <input checked="" type="checkbox"/> | <input type="checkbox"/> Animals and other organisms   |
| <input checked="" type="checkbox"/> | <input type="checkbox"/> Human research participants   |
| <input checked="" type="checkbox"/> | <input type="checkbox"/> Clinical data                 |
| <input checked="" type="checkbox"/> | <input type="checkbox"/> Dual use research of concern  |

### Methods

- |                                     |   |
|-------------------------------------|---|
| n/a                                 | Involved in the study                           |
| <input type="checkbox"/>            | <input checked="" type="checkbox"/> ChIP-seq    |
| <input checked="" type="checkbox"/> | <input type="checkbox"/> Flow cytometry         |
| <input checked="" type="checkbox"/> | <input type="checkbox"/> MRI-based neuroimaging |

## Antibodies

### Antibodies used

Antibody for immunoprecipitation and mass spectrometry: anti-Flag M2 Affinity Gel (A2220; Sigma-Aldrich; monoclonal; 1:200 dilution);  
Antibodies for ChIP-seq: Anti-GFP (Ab290; Abcam; polyclonal; 1:600 dilution);  
Antibodies for Western blot: Anti-GST (M20007L; Abmart; monoclonal; 1:5000 dilution)

### Validation

The antibodies have been validated according to manufacturer's instructions. Western blotting was used to determine the expression of tagged transgenes in corresponding transgenic plants.

## ChIP-seq

### Data deposition

- Confirm that both raw and final processed data have been deposited in a public database such as [GEO](#).
- Confirm that you have deposited or provided access to graph files (e.g. BED files) for the called peaks.

### Data access links

*May remain private before publication.*

<https://www.ncbi.nlm.nih.gov/geo/query/acc.cgi?acc=GSE193397>

### Files in database submission

GSM5777239	BRD1-GFP, Input
GSM5777240	BRD1-GFP, IP, rep1
GSM5777241	BRD1-GFP, IP, rep2
GSM5777242	SWI3C-GFP, Input
GSM5777243	SWI3C-GFP, IP, rep1
GSM5777244	SWI3C-GFP, IP, rep2
GSM5777245	SYD-GFP, Input
GSM5777246	SYD-GFP, IP, rep1
GSM5777247	SYD-GFP, IP, rep2
GSM5777248	SWI3D-GFP, Input
GSM5777249	SWI3D-GFP, IP, rep1
GSM5777250	SWI3D-GFP, IP, rep2
GSM5777251	SYS1-GFP, Input
GSM5777252	SYS1-GFP, IP, rep1
GSM5777253	SYS1-GFP, IP, rep2
GSM5777254	MINU2-GFP, Input
GSM5777255	MINU2-GFP, IP, rep1
GSM5777256	MINU2-GFP, IP, rep2
GSM5777257	PMS2B-GFP, Input
GSM5777258	PMS2B-GFP, IP, rep1
GSM5777259	PMS2B-GFP, IP, rep2

## Methodology

Replicates	All the experiments were biologically repeated and similar results were obtained.
Sequencing depth	At least 60 X coverage for the Arabidopsis genome; all reads were pair-ends (150 bp X2).
Antibodies	Anti-GFP (Ab290; Abcam)
Peak calling parameters	Sequences were aligned to Arabidopsis genome Tair10 using Bowtie2 (v2.3.5.1) with default parameters. Peak calling were done by MACS2 (v2.2.7.1) using the parameters of '-f BAMPE -g 119145879 -bdg -nomodel -c input.bam'.
Data quality	Adapters and low-quality reads were removed, and the clean reads were mapped to the Arabidopsis genome (TAIR10). Input samples were used as a control. For further analysis, only the peaks that were present in both replicates (irreproducible discovery rate≤0.05) were considered.
Software	ChIP-seq data were analyzed using Bowtie2 (v2.3.5.1), MACS2 (v2.2.7.1) and DeepTools (v3.4.3).